



RESEARCH ARTICLE

How Merkel cells transduce mechanical stimuli: A biophysical model of Merkel cells

Fangtao Mao , Wenzhen Yang *

Research Center for Humanoid Sensing, Intelligent Perception Research Institute of Zhejiang Lab, Hangzhou, Zhejiang, China

* ywz@zhejianglab.edu.cn

Abstract

Merkel cells combine with $A\beta$ afferents, producing slowly adapting type 1 (SA1) responses to mechanical stimuli. However, how Merkel cells transduce mechanical stimuli into neural signals to $A\beta$ afferents is still unclear. Here we develop a biophysical model of Merkel cells for mechanical transduction by incorporating main ingredients such as Ca^{2+} and K^+ voltage-gated channels, *Piezo2* channels, internal Ca^{2+} stores, neurotransmitters release, and cell deformation. We first validate our model with several experiments. Then we reveal that Ca^{2+} and K^+ channels on the plasma membrane shape the depolarization of membrane potentials, further regulating the Ca^{2+} transients in the cells. We also show that Ca^{2+} channels on the plasma membrane mainly inspire the Ca^{2+} transients, while internal Ca^{2+} stores mainly maintain the Ca^{2+} transients. Moreover, we show that though *Piezo2* channels are rapidly adapting mechanical-sensitive channels, they are sufficient to inspire sustained Ca^{2+} transients in Merkel cells, which further induce the release of neurotransmitters for tens of seconds. Thus our work provides a model that captures the membrane potentials and Ca^{2+} transients features of Merkel cells and partly explains how Merkel cells transduce the mechanical stimuli by *Piezo2* channels.

 OPEN ACCESS

Citation: Mao F, Yang W (2023) How Merkel cells transduce mechanical stimuli: A biophysical model of Merkel cells. *PLoS Comput Biol* 19(12): e1011720. <https://doi.org/10.1371/journal.pcbi.1011720>

Editor: Hugues Berry, Inria, FRANCE

Received: July 2, 2023

Accepted: November 27, 2023

Published: December 20, 2023

Copyright: © 2023 Mao, Yang. This is an open access article distributed under the terms of the [Creative Commons Attribution License](https://creativecommons.org/licenses/by/4.0/), which permits unrestricted use, distribution, and reproduction in any medium, provided the original author and source are credited.

Data Availability Statement: All relevant data are within the manuscript, and [Supporting information files](#).

Funding: This work was supported by Youth Fund of the Zhejiang Lab (K2023MG0AA02 to FM, K2023MG0AA11), the National Key Research and Development Program of China (2021YFF0600203 to WY), the Key Research Project of the Zhejiang Lab (K2022PG1BB01 to WY, 2022MG0AC04 to WY). The funders had no role in study design, data collection and analysis, decision to publish, or preparation of the manuscript.

Author summary

Touch is an essential way for humans to sense the physical world. It is necessary to figure out how our tactile system works. However, how Merkel cells convey mechanical stimuli into neural signals and deliver them to $A\beta$ afferents is still poorly understood. In this work, we develop a biophysical model of Merkel cells for mechanical transduction. We show that Ca^{2+} and K^+ channels on the plasma membrane control the membrane potentials of Merkel cells and further regulate the Ca^{2+} transients in the cells. Ca^{2+} channels on ER and MT directly contribute to the Ca^{2+} transients. Under indentation, the influx of Ca^{2+} through *Piezo2* channels is sufficient to trigger the Ca^{2+} transients in Merkel cells and internal Ca^{2+} stores inherit to maintain the Ca^{2+} transients, which further result in a sustained release of neurotransmitters that activates the $A\beta$ afferents. Thus our findings partly explain how Merkel cells combine with $A\beta$ afferents to generate an SA1 response to sustained indentation by *Piezo2* channels.

Competing interests: The authors have declared that no competing interests exist.

Introduction

Tactile end organs transduce various mechanical stimuli into action potential sequences. Among them, Merkel cell-neurite complexes, which mainly produce slowly adapting type 1 (SA1) responses [1–3], play an important role in the reception of corners, edges, curvatures of objects, and gentle touch [4, 5].

Merkel cell-neurite complexes generate sustained action potentials with irregular intervals when a sustained mechanical stimulus is applied to the skin [3, 6, 7]. Recent studies found that *Piezo2* channels, which are expressed in Merkel cells and $A\beta$ afferents and only generate a transient current, are necessary for the sustained firing of $A\beta$ afferents [7–9]. However, continuous current injections are required for $A\beta$ afferents to generate sustained action potentials [3, 10]. Recent theoretical research also thought that rapidly adapting (RA) mechanical-sensitive (MS) channels like *Piezo2* cannot account for the sustained responses of Merkel cell-neurite complexes [11]. Therefore, how Merkel cells transduce the mechanical stimuli with *Piezo2* channels has not been well revealed.

Recent studies found that Merkel cells express many molecules that mediate synaptic vesicle release [12–14]. Some studies further checked that Merkel cells release neurotransmitter analogs to $A\beta$ afferents [15, 16]. Merkel cells also generate unique Ca^{2+} transients under mechanical stimuli [6, 17]. Ca^{2+} is an important signal that regulates the release of neurotransmitters [18–20]. Besides, different from other neural cells, Merkel cells do not generate the Na^+ -related action potentials but have the Ca^{2+} and K^+ dominant membrane potential behaviors [17, 21–23]. Finally, *Piezo2* channels transport ions into the cell under mechanical stimulus, with a preferential transport of Ca^{2+} . Therefore, *Piezo2* channels, membrane potentials, Ca^{2+} transients, and vesicles release together to form a line in Merkel cells to translate the mechanical stimulus. However, a detailed biophysical model of Merkel cells is still lacking. It is still unclear how these parameters participate in the mechanical transduction of Merkel cells.

To address these questions, we establish a biophysical electrophysiological model of Merkel cells. First, we validate our model with experiments of [21–24]. The membrane potentials of Merkel cells under current stimuli vary with the conductances of plasma membrane Ca^{2+} channels. The Ca^{2+} transients in Merkel cells under high K^+ solutions and hypotonic shock last for tens of seconds. Then, we explore the roles of ion channels on the plasma membrane, endoplasmic reticulum (ER), and mitochondria (MT) in membrane potentials and Ca^{2+} transients regulations of Merkel cells. The results show that $Ca_v1.2$ channels mainly contribute to the form of the peak of membrane potentials, while $K_v1.4$ channels inhibit this peak. *BKCa*, *KDR*, and $Ca_v2.1$ channels mainly regulate the steady membrane potentials. $Ca_v1.2$ channels cause the increase of Ca^{2+} concentration at the initial time, while $Ca_v2.1$ channels, Ryanodine and IP_3 receptors on the ER increase the duration of Ca^{2+} transients. Interestingly, the Ca^{2+} channels on MT also lengthen the Ca^{2+} transients by satisfying the peak of Ca^{2+} transients.

Based on the above results, we further study the mechanical transduction of Merkel cells with *Piezo2* channels. The results show that Merkel cells generate a continuous neurotransmitter release under a sustained indentation, in which the duration of neurotransmitter release is positively related to indentation depth. This duration lasts for tens of seconds, corresponding to the firing time of Merkel discs under indentation [6, 7, 24]. These results can partly explain how *Piezo2* channels (RA MS channels) inspire Merkel cells to have the sustained neurotransmitter excitation on $A\beta$ afferents for their continuous firing.

Materials and methods

Kinetics of ions

Most Merkel cells are globular in shape [25], and some Merkel cells in hair follicles have an irregular shape [24]. To simplify, here we assume the Merkel cell is a sphere with a radius of r . Merkel cells contain Na^+ , K^+ , Cl^- , Ca^{2+} , and some micro-molecules A^- with negative charges inside the cell. Generally, cells keep in a near electro-neutral condition [26, 27]. We denote n_{Na} , n_K , n_{Cl} , n_{Ca} , and n_A as the mole numbers of Na^+ , K^+ , Cl^- , Ca^{2+} , and A^- inside the cell, respectively. Then their concentrations are $C_{Na} = n_{Na}/(V - V_{ER} - V_{MT})$, $C_K = n_K/(V - V_{ER} - V_{MT})$, $C_{Cl} = n_{Cl}/(V - V_{ER} - V_{MT})$, $C_{Ca} = n_{Ca}/(V - V_{ER} - V_{MT})$, $C_A = n_A/(V - V_{ER} - V_{MT})$, where V is the volume of Merkel cells, $V = 4/3\pi r^3$, V_{ER} and V_{MT} are Endoplasmic reticulum and Mitochondria volume. We also set $C_{Na,out}$, $C_{K,out}$, $C_{Cl,out}$ and $C_{Ca,out}$ as Na^+ , K^+ , Cl^- , and Ca^{2+} concentrations in environmental solutions, respectively. Ions inside the cell are regulated by ion channels embedded in the cell membrane.

K^+ channels. The molecular profiling of Merkel cells shows that they express three kinds of voltage-gated K^+ channels: $K_v4.2$, $K_v1.4$, and $K_v8.1$ [12]. However, the study of Yamashita shows there are only two kinds of ion currents of K^+ in Merkel cells, which are similar to currents of $K_v4.2$ and $K_v1.4$ [21]. Further studies elucidated that $K_v8.1$ channels do not generate ion currents directly but regulate other K^+ channels' activities indirectly [28]. Therefore, here we only consider $K_v4.2$ and $K_v1.4$ channels in Merkel cells.

$K_v1.4$ channels. $K_v1.4$ channels are activated rapidly with the increase of cell membrane potential. A part of the currents inactivates rapidly, while the remaining currents have a slower inactivation [21, 29]. The data for modeling $K_v1.4$ channels was obtained by fitting the data from [29] (Fig B in S1 Appendix),

$$J_{K_v1.4} = -g_{K_v1.4} m^4 (0.7h_{fast} + 0.3h_{slow})(V_m - E_K)/F, \tag{1}$$

where $g_{K_v1.4}$ is the specific membrane conductance of $K_v1.4$, V_m is the membrane potential, E_K is the equilibrium (or Nernst) potential of K^+ , F is the Faraday constant. For m , h_{fast} and h_{slow} [29],

$$\frac{dm}{dt} = \frac{m_\infty - m}{\tau_m}, \tag{2}$$

$$m_\infty = \frac{1}{1 + \exp\left(-\frac{V_m + 23.12}{11.46}\right)}, \tag{3}$$

$$\tau_m = 0.6 + \exp\left(-\frac{V_m + 12.02}{25.87}\right), \tag{4}$$

$$\frac{dh_{fast}}{dt} = \frac{h_\infty - h_{fast}}{\tau_{h,fast}}, \tag{5}$$

$$h_{\infty} = \frac{1}{1 + \exp\left(\frac{V_m + 44.36}{2.73}\right)}, \tag{6}$$

$$\tau_{h,fast} = -0.1086 \cdot V_m + 48.67, \tag{7}$$

$$\frac{dh_{slow}}{dt} = \frac{h_{\infty} - h_{slow}}{\tau_{h,slow}}, \tag{8}$$

$$\tau_{h,slow} = 17.28. \tag{9}$$

K_v4.2 channels. *K_v4.2* channels are both activated and inactivated rapidly [21, 30]. The model data was obtained from [21] (Fig C in S1 Appendix),

$$J_{K_v4.2} = -g_{K_v4.2} m h (V_m - E_K) / F, \tag{10}$$

where $g_{K_v4.2}$ is the specific membrane conductance of *K_v4.2*. For m, h ,

$$\frac{dm}{dt} = \frac{m_{\infty} - m}{\tau_m}, \tag{11}$$

$$m_{\infty} = \frac{1}{1 + \exp\left(-\frac{V_m - 17.66}{22.75}\right)}, \tag{12}$$

$$\tau_m = 3 + 2 \exp\left(-\frac{V_m - 19.68}{41.23}\right), \tag{13}$$

$$\frac{dh}{dt} = \frac{h_{\infty} - h}{\tau_h}, \tag{14}$$

$$h_{\infty} = \frac{1}{1 + \exp\left(\frac{V_m + 44.36}{2.73}\right)}, \tag{15}$$

$$\tau_h = 10 + \exp\left(-\frac{V_m - 488}{165.84}\right). \tag{16}$$

In addition to the above two K^+ channels, there are also Ca^{2+} -activated K^+ channels (BK_{Ca} channels) and Delayed-rectifier K channels (KDR channels) in Merkel cells [12, 21, 23]. These two kinds of channels carry the majority of K^+ currents in Merkel cells [21, 23].

BK_{Ca} channels. *BK_{Ca}* channels are activated by membrane potential and have no obvious inactivation behavior. As the intracellular Ca^{2+} concentration increases, the curve of the channels' open probability versus membrane potential has a right shift [23, 31]. Here we take a similar channel model from [32],

$$J_{BK_{Ca}} = -g_{BK_{Ca}} n (V_m - E_{BK_{Ca}}) / F, \tag{17}$$

where $g_{BK_{Ca}}$ is the specific membrane conductance of BK_{Ca} , $E_{BK_{Ca}}$ is the Nernst potential, For n ,

$$\frac{dn}{dt} = \frac{n_{\infty} - n}{\tau_n}, \tag{18}$$

$$pCa = \log \frac{C_{Ca}}{K_{BK_{Ca}}}, \tag{19}$$

$$V_{half} = -43.3pCa - 110, \tag{20}$$

$$sf = 33.88 \exp\left(-\left(\frac{pCa + 5.42}{2.2}\right)^2\right), \tag{21}$$

$$n_{\infty} = \frac{1}{1 + \exp\left(-\frac{V_m - V_{half}}{sf}\right)}, \tag{22}$$

$$\tau_n = 0.75 + 5.55 \exp\left(\frac{V_m}{42.91}\right) - 0.12V_m, \tag{23}$$

where $K_{BK_{Ca}} = 1mM$.

KDR channels present a slow activation behavior, the parameters are taken from [21] (Fig D in [S1 Appendix](#)),

$$J_{KDR} = -g_{KDR}n(V_m - E_{KDR})/F, \tag{24}$$

where g_{KDR} is the specific membrane conductance of KDR , E_{KDR} is the Nernst potential, For n ,

$$\frac{dn}{dt} = \frac{n_{\infty} - n}{\tau_n}, \tag{25}$$

$$n_{\infty} = \frac{1}{1 + \exp\left(-\frac{V_m + 33.3}{8.7}\right)}, \tag{26}$$

$$\tau_n = 2.2 + 20 \exp\left(-\left(\frac{V_m + 13.03}{29.55}\right)^2\right). \tag{27}$$

Ca²⁺ channels. Ca^{2+} plays an important role in Merkel cells' responses under different stimuli like mechanical stimulation, hypotonic shock, etc [12, 22, 23]. Merkel cells mainly express two kinds of voltage-gated Ca^{2+} channels: $Ca_v1.2$ and $Ca_v2.1$ [12].

$Ca_v1.2$ channels. $Ca_v1.2$ channels are L-type(long-lasting) channels, which exhibit a Ca^{2+} -dependent inactivation [33, 34]. The equations were taken from [32],

$$J_{Ca_v1.2} = -g_{Ca_v1.2}mh \cdot hCa(V_m - E_{Ca})/F, \tag{28}$$

where $g_{Ca_v1.2}$ is the specific membrane conductance of $Ca_v1.2$, E_{Ca} is the Nernst potential, for

m , h , and hCa ,

$$\frac{dm}{dt} = \frac{m_\infty - m}{\tau_m}, \tag{29}$$

$$m_\infty = \frac{1}{1 + \exp\left(-\frac{V_m - 8.46}{4.26}\right)}, \tag{30}$$

$$\tau_m = 2.11 + 3.86 \exp\left(-2\left(\frac{V_m + 10}{16.02}\right)^2\right), \tag{31}$$

$$\frac{dh}{dt} = \frac{h_\infty - h}{\tau_h}, \tag{32}$$

$$h_\infty = \frac{1}{1 + \exp\left(\frac{V_m + 42.52}{7.48}\right)}, \tag{33}$$

$$\tau_h = 825.80 + 637.91 \exp\left(-2\left(\frac{V_m}{39.75}\right)^2\right), \tag{34}$$

$$hCa = \frac{1}{1 + \left(\frac{C_{Ca}}{K_{hCa}}\right)^4}, \tag{35}$$

where $K_{hCa} = 1\mu M$.

Ca_v2.1 channels. Ca_v2.1 channels are P/Q-type channels [33, 35], which have no obvious inactivation behavior. The equations were taken from [32],

$$J_{Ca_v2.1} = -g_{Ca_v2.1}n(V_m - E_{Ca})/F, \tag{36}$$

where $g_{Ca_v2.1}$ is the specific membrane conductance of Ca_v2.1, E_{Ca} is the Nernst potential, for n ,

$$\frac{dn}{dt} = \frac{n_\infty - n}{\tau_n}, \tag{37}$$

$$n_\infty = \frac{1}{1 + \exp\left(-\frac{V_m + 5.1}{3.1}\right)}, \tag{38}$$

$$\tau_n = 0.35 + 5.51 \exp\left(-2\left(\frac{V_m + 9.73}{18.14}\right)^2\right). \tag{39}$$

Piezo2 channels. Merkel cells cannot translate mechanical stimuli to neural signals without Piezo2 channels, which carry inward currents under the indentation [6, 7]. Piezo2 channels are mechanical-sensitive(MS) channels, which can also be opened by the microtubule suction

of the membrane [36–38]. Therefore we assume that *Piezo2* channels' open probability is regulated by membrane tension. Given that cells have a cortex which is comprised of the cell membrane and a thin, cross-linked actin network lying beneath the membrane, we assume that *Piezo2* channels open probability is regulated by the cortex stress σ [39]. *Piezo2* channels exhibit a fast activation and a fast inactivation [36, 40]. Besides, *Piezo2* channels have another inactivation with a much longer time scale [38]. Here we introduce C , O , In , and h_{slow} to represent the channel closed state, open state, short-time inactivation state, and the state beyond long-time inactivation, respectively. Only channels beyond the long-time inactivation state and open state can transport ions. The data for modeling *Piezo2* channels was obtained by fitting the data from [36],

$$J_{Piezo2} = -g_{Piezo2} O h_{slow} (V_m - E_{Piezo2}) / F, \quad (40)$$

where J_{Piezo2} is specific membrane conductance of *Piezo2* channels, E_{Piezo2} is the Nernst potential. Under loading,

$$\frac{dC}{dt} = \frac{C_\infty - C}{\tau_C}, \quad (41)$$

$$\frac{dO}{dt} = -\frac{O}{\tau_O} - \frac{C_\infty - C}{\tau_C}, \quad (42)$$

$$\frac{dIn}{dt} = \frac{O}{\tau_O}. \quad (43)$$

Under unloading,

$$\frac{dC}{dt} = -\frac{In_\infty - In}{\tau_{In}}, \quad (44)$$

$$\frac{dIn}{dt} = \frac{In_\infty - In}{\tau_{In}}. \quad (45)$$

Other parameters are the same all the time.

$$\frac{dh_{slow}}{dt} = \frac{h_{slow,\infty} - h_{slow}}{\tau_{h_{slow}}}, \quad (46)$$

$$C_{\infty} = \frac{1}{1 + \exp\left(\frac{\sigma - \sigma_{s1}}{\sigma_{f1}}\right)}, \quad (47)$$

$$\tau_c = 0.5 + \frac{1.5}{1 + \exp\left(-\frac{\sigma - \sigma_{s2}}{\sigma_{f2}}\right)}, \quad (48)$$

$$\tau_o = 2.5 + \frac{5.5}{1 + \exp\left(-\frac{\sigma - \sigma_{s4}}{\sigma_{f4}}\right)}, \quad (49)$$

$$In_{\infty} = \frac{1}{1 + \exp\left(-\frac{\sigma - \sigma_{s1}}{\sigma_{f1}}\right)}, \quad (50)$$

$$\tau_{In} = 0.5 + \frac{1.5}{1 + \exp\left(-\frac{\sigma - \sigma_{s2}}{\sigma_{f2}}\right)}, \quad (51)$$

$$h_{slow,\infty} = \frac{1}{1 + \exp\left(-\frac{\sigma - \sigma_{s7}}{\sigma_{f7}}\right)}, \quad (52)$$

$$\tau_{h_{slow}} = \frac{150}{1 + \exp\left(\frac{\sigma - \sigma_{s8}}{\sigma_{f8}}\right)}. \quad (53)$$

The parameters of *Piezo2* channels are listed in [Table 1](#), and the specific descriptions of *Piezo2* channels are seen in Parameters estimation in [S1 Appendix](#). The currents through *Piezo2* channels in simulation and experiments are shown in [Fig 1](#).

Piezo2 channels are non-selective anion channels [36, 40]. All Ca^{2+} , K^+ , and Na^+ could flow across *Piezo2* channels. But Ca^{2+} has the highest priority [36, 40]. Therefore, we assumed that the currents across *Piezo2* channels are Ca^{2+} currents.

Table 1. Parameters of Piezo2 channels.

Parameter	Description	Value in simulation(ref)
σ_{s1}	Midpoint cortex stress of C (Pa)	1450 [36]
σ_{f1}	Reference cortex stress of C (Pa)	120 [36]
σ_{s2}	Midpoint cortex stress of the time constant for C (Pa)	1450 [36]
σ_{f2}	Reference cortex stress of the time constant for C (Pa)	40 [36]
σ_{s4}	Midpoint cortex stress of the time constant for O (Pa)	1450 [36]
σ_{f4}	Reference cortex stress of the time constant for O (Pa)	100 [36]
σ_{s7}	Midpoint cortex stress of h_{slow} (Pa)	1450 [41]
σ_{f7}	Reference cortex stress of h_{slow} (Pa)	200 [41]
σ_{s8}	Midpoint cortex stress of the time constant for h_{slow} (Pa)	1450 [41]
σ_{f8}	Reference cortex stress of the time constant for h_{slow} (Pa)	2000 [41]
g_{Piezo2}	Specific membrane conductance of Piezo2(mS/cm ²)	3 [7]
E_{Piezo2}	Nernst potential (mV)	6 [36, 40]

<https://doi.org/10.1371/journal.pcbi.1011720.t001>

Besides these channels above, Merkel cells have a passive electrical property. We take Na^+ , K^+ , Cl^- , and Ca^{2+} leak channels into consideration. These leak ions flow can be written as

$$J_{Na,leak} = -\frac{1}{F}g_{Na,leak}(V_m - E_{Na}), \tag{54}$$

$$J_{K,leak} = -\frac{1}{F}g_{K,leak}(V_m - E_K), \tag{55}$$

$$J_{Cl,leak} = \frac{1}{F}g_{Cl,leak}(V_m - E_{Cl}), \tag{56}$$

$$J_{Ca,leak} = \frac{1}{F}g_{Ca,leak}(V_m - E_{Ca}), \tag{57}$$

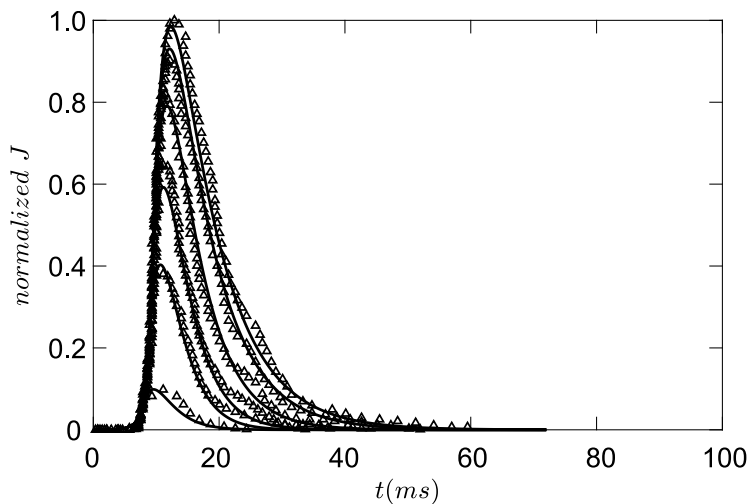


Fig 1. Piezo2 channels. The ions flow generated in Piezo2 channels under different indentation depths. triangle line: experimental results from [36], solid line: simulation results($d_0 = 5.8\mu m, d_0 = 6.7\mu m, d_0 = 7.0\mu m, d_0 = 7.3\mu m, d_0 = 7.6\mu m, d_0 = 7.9\mu m$).

<https://doi.org/10.1371/journal.pcbi.1011720.g001>

where $g_{i,leak}$ and E_i are the specific membrane conductance and the equilibrium (or Nernst) potential of i , $E_i = -\frac{RT}{z_i F} \ln \frac{C_i}{C_{i,out}}$, R is the gas constant, T is the thermodynamic temperature, z_i is the valence of ions, $i = Na^+, K^+, Cl^-, Ca^{2+}$.

Pumps, cotransporters, and exchangers. Similar to most cells, Merkel cells also contain ion pumps, cotransporters, and exchangers to keep the ions' balance inside the cell. Here we take Na^+/K^+ pumps, $Na^+/K^+/Cl^-$ cotransporters, K^+/Cl^- cotransporters, Na^+/Ca^{2+} exchangers, and Ca^{2+} pumps on the plasma membrane into consideration.

Na^+/K^+ pumps, which transport two K^+ into the cell and three Na^+ out of the cell once by consuming energy, keep a high K^+ concentration and a low Na^+ concentration in the cell [42, 43]. The intracellular concentrations of Na^+ and K^+ affect the rate of Na^+/K^+ pumps [44, 45],

$$J_{NaKpump} = P_{NaKpump} \frac{1}{(1 + K_{Na,NaK}/C_{Na})^3} \frac{1}{(1 + C_K/K_{K,NaK})^2}, \tag{58}$$

where $P_{NaKpump}$ is rate constant. $K_{Na,NaK}$ and $K_{K,NaK}$ are constants, $K_{Na,NaK} = 10mM$, $K_{K,NaK} = 140mM$ [46].

$Na^+/K^+/Cl^-$ cotransporters, which transport one Na^+ , one K^+ , and two Cl^- in the same direction once, mainly loading Cl^- into the cell [47–49]. Their flow is controlled by three ions concentrations [27],

$$J_{NKCC1} = P_{NKCC1} (C_{Na,out} C_{K,out} C_{Cl,out}^2 - C_{Na} C_K C_{Cl}^2), \tag{59}$$

where P_{NKCC1} is the rate constant.

K^+/Cl^- cotransporters, which transport one K^+ and one Cl^- in the same direction once, mainly extruding Cl^- from inside the cell [48]. Their flow was regulated by the Cl^- and K^+ concentrations across the membrane [50–52],

$$J_{KCC2} = P_{KCC2} \frac{C_{Cl}}{C_{Cl,out}} \frac{C_K}{C_{K,out}}, \tag{60}$$

where P_{KCC2} is the rate constant.

Plasma membrane Ca^{2+} pumps and Na^+/Ca^{2+} exchangers both help to eliminate Ca^{2+} from inside the cell [53, 54]. A general model of Ca^{2+} pumps was used [55],

$$J_{Capump} = P_{Capump} \frac{C_{Ca}^2}{C_{Ca}^2 + K_{Capump}^2}, \tag{61}$$

where P_{Capump} is the rate constant, K_{Capump} is constant, $K_{Capump} = 0.3uM$.

Na^+/Ca^{2+} exchangers exhibit complex dynamic behavior. They are motivated by membrane potential, Ca^{2+} and Na^+ concentrations. Under steady state, Na^+/Ca^{2+} exchangers transport Ca^{2+} outside the cell. When the cell is stimulated by currents or membrane voltage, the direction of Na^+/Ca^{2+} exchangers flow will be reversed [56, 57]. The dynamic equation of Na^+/Ca^{2+} exchangers can be written as [57],

$$J_{Cana} = P_{Cana} \frac{1}{K_{mNa}^3 + C_{Na,out}^3} \frac{1}{K_{mCa} + C_{Ca,out}} \frac{1}{1 + ksat \cdot \exp(\eta - 1) V_m F / (RT)} \cdot \exp\left(\eta V_m \frac{F}{RT}\right) C_{Na}^3 C_{Ca,out} - \exp\left((\eta - 1) V_m \frac{F}{RT}\right) C_{Na,out}^3 C_{Ca}, \tag{62}$$

where P_{Cana} is the rate constant, K_{mNa} and K_{mCa} are constants, $K_{mNa} = 87.5mM$, $K_{mCa} = 0.5uM$, $\eta = 0.1$, $ksat = 0.35$ [57].

Internal Ca^{2+} dynamics

Intracellular Ca^{2+} sources also play an important role in Ca^{2+} regulation in Merkel cells. The elimination of internal Ca^{2+} store greatly reduces the Ca^{2+} transients [22, 23].

Endoplasmic reticulum and Mitochondria are the main internal Ca^{2+} stores. There are main three channels on the Endoplasmic reticulum (ER) membrane including Ca^{2+} ATPase pump, Inositol 1,4,5-trisphosphate receptor (IP_3 receptor), and Ryanodine receptor. Ca^{2+} ATPase pumps consume energy to actively load Ca^{2+} into endoplasmic reticulum, and their rate increase with cytoplasmic Ca^{2+} concentration [58, 59]

$$J_{pump,ER} = P_{pump,ER} \frac{C_{Ca}^2}{C_{Ca}^2 + K_{ERpump}^2}, \tag{63}$$

where $P_{pump,ER}$ is the rate constant, K_{ERpump} is the dissociation constant, and their values are listed in Table 2.

Ryanodine receptors and IP_3 receptors involve in Ca^{2+} -induced Ca^{2+} release in Merkel cells [22, 23]. The Ca^{2+} flux by Ryanodine receptor is defined by the equation,

$$J_{RYR} = \begin{cases} P_{RYR} \frac{1}{1 + \exp\left(\frac{C_{Ca} - K_{s,RYR}}{K_{f,RYR}}\right)} (C_{Ca,ER} - C_{Ca}), & C_{Ca} > K_{s,RYR} \\ 0, & C_{Ca} \leq K_{s,RYR} \end{cases} \tag{64}$$

where P_{RYR} is the rate constant, $K_{s,RYR}$ and $K_{f,RYR}$ are constant.

Table 2. Parameters of internal Ca^{2+} channels.

Parameter	Description	Value in simulation(ref)
K_{ERpump}	Dissociation constant (μM)	0.1 [59]
$K_{s,RYR}$	Midpoint Ca^{2+} concentration for RYR (μM)	0.3 (Tuned)
$K_{f,RYR}$	Reference Ca^{2+} concentration for RYR (μM)	0.04 (Tuned)
K_{s,IP_3}	Midpoint Ca^{2+} concentration for IP_3 receptors (μM)	0.4 [60, 61]
K_{f1,IP_3}	Reference Ca^{2+} concentration for IP_3 receptors (μM)	0.04 [60, 61]
K_{s2,IP_3}	Midpoint Ca^{2+} concentration for IP_3 receptors (μM)	0.6 [60, 61]
K_{f2,IP_3}	Reference Ca^{2+} concentration for IP_3 receptors (μM)	0.04 [60, 61]
$K_{s,preIP_3}$	Midpoint $preIP_3$ concentration (μM)	5 [63]
$K_{f,preIP_3}$	Reference $preIP_3$ concentration (μM)	1 [63]
τ_m	time constant (ms)	10000 [22, 23]
τ_h	time constant (ms)	20000 [22, 23]
K_{IP_3}	Dissociation constant (μM)	3 [60]
K_{IP_3Ca}	Dissociation constant (μM)	0.5 [63]
S_{ER}	Surface of ER (μm^2)	150 [66]
V_{ER}	Volume of ER (μm^3)	100 [66]
k_{preIP_3}	rate constant ($mol/(cm^3 \cdot ms)$)	10^{-12} (Tuned)
k_{IP_3}	rate constant (1/ms)	4×10^{-5} [63]
k_{dIP_3}	rate constant (1/ms)	2×10^{-5} [63]
K_{MCU}	Dissociation constant (μM)	0.6 [67]
K_{MNCX}	Dissociation constant (μM)	1 (Tuned)
S_{MT}	Surface of mitochondria (μm^2)	150 [66]
V_{MT}	Volume of mitochondria (μm^3)	10 [66]

<https://doi.org/10.1371/journal.pcbi.1011720.t002>

IP_3 receptors have three sites for the combination of Ca^{2+} and IP_3 . One site is for activated Ca^{2+} , and one site is for inhibitory Ca^{2+} [60]. It means that the increase of Ca^{2+} concentration from a low level, the combination of Ca^{2+} to IP_3 receptors activates the receptor, as the Ca^{2+} concentration increase to a very high level, the receptor will be inhibited [61]. We introduce m and h to represent the activation and inhibitory role of Ca^{2+} on IP_3 receptor,

$$\frac{dm}{dt} = \frac{m_\infty - m}{\tau_m}, \tag{65}$$

$$\frac{dh}{dt} = \frac{h_\infty - m}{\tau_h}, \tag{66}$$

where τ_m and τ_h are time constants.

$$m_\infty = \frac{1}{1 + \exp\left(-\frac{C_{Ca} - K_{s1,IP_3}}{K_{f1,IP_3}}\right)}, \tag{67}$$

$$h_\infty = \frac{1}{1 + \exp\left(\frac{C_{Ca} - K_{s2,IP_3}}{K_{f2,IP_3}}\right)}. \tag{68}$$

The remaining site is for IP_3 , and the increase of IP_3 concentration enhances the currents of IP_3 receptors [61]. Thus we assume that IP_3 receptors' open probability equals to

$$J_{ER} = \left(P_{leak} + P_{IP_3} \frac{C_{IP_3}^3}{C_{IP_3}^3 + K_{IP_3}^3} mh \right) (C_{Ca,ER} - C_{Ca}), \tag{69}$$

where P_{leak} and P_{IP_3} are rate constants, P_{leak} represents the leak flow of Ca^{2+} on ER. K_{IP_3} is the dissociation constant, $C_{Ca,ER}$ is the concentration of Ca^{2+} in ER.

IP_3 mobilizes Ca^{2+} from intracellular stores through the IP_3 receptors [62], and itself also takes a dynamic regulation in a single cell [63]. Generally, the entry of Ca^{2+} through Ca^{2+} channels on the membrane cause the hydrolyzation of phosphatidylinositol 4,5-bisphosphate (PIP_2), which produces IP_3 [64]. Then IP_3 will convert to other matters even though the Ca^{2+} concentration is still high [63]. Therefore, we assume the production rate of IP_3 increases with the Ca^{2+} concentration and the conversion rate of IP_3 depends on its concentration,

$$\frac{dC_{IP_3}}{dt} = k_{IP_3} \frac{C_{Ca}^2}{C_{Ca}^2 + K_{IP_3Ca}} C_{preIP_3} - k_{dIP_3} C_{IP_3}, \tag{70}$$

where k_{IP_3} and k_{dIP_3} are the rate constants, K_{IP_3Ca} is the dissociation constant, c_{preIP_3} is the concentration of IP_3 precursors like IP_2 [64].

$preIP_3$ will be also replenished after consumption, and keep a rather stable state [65]. So we assume that $preIP_3$ has a production rate related to its concentration. Then the change of $preIP_3$ will be

$$\frac{dC_{preIP_3}}{dt} = \frac{k_{preIP_3}}{1 + \exp\left(\frac{C_{preIP_3} - K_{s,preIP_3}}{K_{f,preIP_3}}\right)} - k_{IP_3} \frac{C_{Ca}^2}{C_{Ca}^2 + K_{IP_3Ca}^2} C_{preIP_3}. \tag{71}$$

According to the above three Ca^{2+} channels, the dynamic equation of Ca^{2+} in ER will be

$$\frac{dn_{Ca,ER}}{dt} = S_{ER}(-J_{ER} - J_{CICR} + J_{Capump,ER}). \tag{72}$$

$$C_{Ca,ER} = n_{Ca,ER}/V_{ER}.$$

There are Mitochondrial uniporter(MCU) and mitochondrial Na^+/Ca^{2+} exchanger (MNCX) on the mitochondrial membrane. MCU takes up Ca^{2+} into Mitochondria while MNCX releases Ca^{2+} from mitochondria to the cytoplasm. The Mitochondrial uniporter dynamics is controlled by the cytoplasm Ca^{2+} concentration [32],

$$J_{MCU} = P_{MCU} \frac{C_{Ca}^{2.3}}{C_{Ca}^{2.3} + K_{MCU}^{2.3}}, \tag{73}$$

where P_{MCU} is the rate constant, K_{MCU} is the dissociation constant.

The dynamics of mitochondrial Na^+/Ca^{2+} exchanger are controlled by mitochondrial Ca^{2+} concentration [32],

$$J_{MNCX} = P_{MNCX} \frac{C_{Ca,MT}}{C_{Ca,MT} + K_{MNCX}}, \tag{74}$$

where P_{MNCX} is the rate constant, K_{MNCX} is the dissociation constant. $c_{Ca,MT}$ is mitochondrial Ca^{2+} concentration, $c_{Ca,MT} = n_{Ca,MT}/V_{MT}$. The dynamic equation of $n_{Ca,MT}$ will be

$$\frac{dn_{Ca,MT}}{dt} = S_{MT}/(1 + \beta_{MT})(-J_{MNCX} + J_{MCU}), \tag{75}$$

where S_{MT} is the mitochondria surface, $\beta_{MT} = 0.3$, which represents the buffer role for Ca^{2+} of mitochondria membrane [32].

According to the above ion channels, the ions change inside the cell can be written as

$$\frac{dn_{Na}}{dt} = S_{ref}(-3J_{NaKpump} + J_{NKCC1} - 3J_{Cana} + J_{Na,leak}), \tag{76}$$

$$\frac{dn_K}{dt} = S_{ref}(J_{Kv1.4} + J_{Kv4.2} + J_{KDR} + J_{BCa} + 2J_{pump} + J_{NKCC1} - J_{KCC2} + J_{K,leak}), \tag{77}$$

$$\frac{dn_{Cl}}{dt} = S_{ref}(2J_{NKCC1} - J_{KCC2} + J_{Cl,leak}), \tag{78}$$

where S_{ref} is the reference surface area of Merkel cell.

$$\begin{aligned} \frac{dn_{Ca}}{dt} &= S_{ref}(J_{Ca,1.2} + J_{Ca,2.1} - J_{Capump} + J_{Cana} - J_{piezo2} + J_{Ca,leak}) \\ &+ S_{ER}(J_{ER} + J_{CICR} - J_{Capump,ER}) + S_{MT}/(1 + \beta_{MT})(J_{MNCX} - J_{MCU}), \end{aligned} \tag{79}$$

The membrane potentials of Merkel cells are regulated by currents across total ion channels. The Na^+/K^+ pumps transport two K^+ into the cell and three Na^+ out of the cell, so there is one charge out of the cell once. The cotransporters transport a Na^+ , a K^+ , and two Cl^- in the same direction once, so the total discharge is zero. The Na^+/Ca^{2+} exchangers transduce three Na^+ into the cell and one Ca^{2+} out of the cell once, so there is one charge out of the cell once.

Then the dynamic equation of V_m is

$$C_m \frac{dV_m}{dt} = (J_{K_v,1.4} + J_{K_v,4.2} + J_{KDR} + J_{BCa} + 2J_{Ca_v,1.2} + 2J_{Ca_v,2.1} + 2J_{piezo2} - J_{NaKpump} - J_{Cana} - 2J_{Capump} + J_{K,leak} + J_{Na,leak} - J_{Cl,leak} + 2J_{Ca,leak})F, \tag{80}$$

where C_m is the specific membrane capacitance.

Volume change

The cell volume V change is dependent on the flow of water across the cell membrane [39]

$$\frac{dV}{dt} = S \cdot J_{water}, \tag{81}$$

where S is the cell surface area, $S = 4\pi r^2$, J_{water} is water flux, it is controlled by the hydrostatic pressure difference and the osmotic pressure difference across the membrane [39]

$$J_{water} = -\alpha(\Delta P - \Delta\Pi), \tag{82}$$

where α is a rate constant $\alpha = 10^{-9} cm \cdot ms^{-1} \cdot Pa^{-1}$, $\Delta\Pi$ is the osmotic pressure difference across the membrane, which can be described as

$$\Delta\Pi = (C_{Na} + C_K + C_{Cl} + C_{Ca} + C_A - C_{Na,out} - C_{K,out} - C_{Cl,out} - C_{Ca,out})RT. \tag{83}$$

Cells have a cortex which is comprised of the cell membrane and a thin, cross-linked actin network lying beneath the membrane. We take the cortex as an elastic layer, the cortex stress satisfies [39]

$$\sigma = \frac{K}{2} \left(\frac{S}{S_{ref}} - 1 \right) - \sigma_a, \tag{84}$$

where K is the cortex elastic modulus, $K = 6000Pa$, S_{ref} represents the cell surface under no stress, σ_a is the active contraction stress produced by the actin network, $\sigma_a = -100Pa$. For a spherical cell, the relationship between the cortex stress and hydrostatic pressure satisfies [39]

$$\Delta P = \frac{2h_c \sigma}{r}, \tag{85}$$

where h_c is the cortex thickness, $h_c = 0.5\mu m$ [39].

Results

Validation of the model

There are three main stimuli to study the properties of Merkel cells, which are current pulses, high K^+ solutions stimuli, and hypotonic shocks [7, 21–23]. We consider these three kinds of situations below.

Current pulses. The rectangular negative current pulses induce the membrane potential dynamics of Merkel cells(Fig 2A and 2B), and the parameters of ion channels are seen in Table 3. The solid lines are simulation results and the triangle lines are experimental results from [21]. The results show that Merkel cells have almost passive responses to negative current pulses(Fig 2B).

However, the membrane properties of Merkel cells under positive current pulses are rather different. As shown in Fig 2C and 2D, when the amplitude of the current pulses is small, the

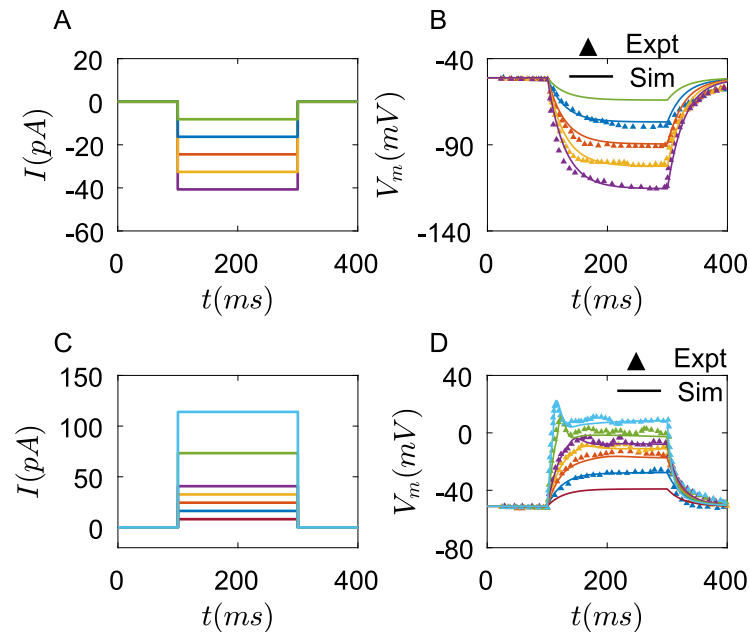


Fig 2. The membrane potential dynamics of one Merkel cell under the rectangular current pulses. (A) Negative current pulses step in 8.14pA (experimental current step in 10pA). (B) Membrane potentials change under negative current pulses. The solid lines are simulation results, and the triangles are experimental results from [21]. (C) Positive current pulses step in 8.14pA, Green line: $9 \times 8.14\text{pA}$, blue line: $14 \times 8.14\text{pA}$. (D) Membrane potentials change under positive current pulses. The solid lines are the simulation results, and the triangles are experimental results from [21]. The parameters of ion channels are seen in Table 3.

<https://doi.org/10.1371/journal.pcbi.1011720.g002>

membrane potential dynamics of Merkel cells are still like a passive response. As the currents increase (green and wathet blue line), the membrane potentials rise rapidly to a peak, then decrease and gradually stabilize. Unlike most other sensory cells or afferents, Merkel cells do not generate action potentials [7, 21].

Some Merkel cells exhibit more complex membrane potential dynamics [24] (Fig 3A). By changing the specific membrane conductance of Ca^{2+} and K^+ channels and rate constants of some pumps on the membrane, we can get similar results. As shown in Fig 3B, the membrane potentials of Merkel cells rapidly reach a step, then fire. Ca^{2+} plays an important role in this membrane potential dynamics. If the Ca^{2+} concentration is reduced in the external solutions, the fire of membrane potentials disappears (Fig 3C and 3D).

Merkel cells not only have membrane potential regulation but also show Ca^{2+} dynamic behaviors. The common stimuli which elicit Ca^{2+} in experiments are high K^+ solutions and hypotonic shock.

High K^+ stimulus. High K^+ solutions are made by reducing Na^+ and increasing K^+ concentrations in external solutions [22, 23]. The experimental results from [23] are shown in Fig 4A. Here we increase $C_{\text{K},\text{out}}$ by 130mM, and reduce $C_{\text{Na},\text{out}}$ by 130mM to represent the high K^+ solution. The results show that the high K^+ solution induces a rapid increase in Ca^{2+} concentration. After reaching a peak, Ca^{2+} concentration decreases slowly (Fig 4B). This Ca^{2+} transient could last for tens of seconds in Merkel cells, which is much longer than the timescale of membrane potential dynamics (Fig 2). This Ca^{2+} transient is regulated by both plasma membrane Ca^{2+} channels and internal Ca^{2+} channels in Merkel cells. The inhibition of ER Ca^{2+} stores causes a dramatic drop in fluorescence intensity of Ca^{2+} (Fig 4C). By setting the rate

Table 3. Parameters differences of ion channels in Figs 2 and 3.

Parameter	Value in Fig 2	Value in Fig 3
$C_m(\mu F/\mu m^2)$	4×10^{-8} [21]	2×10^{-8} [7]
$g_{Kv1.4}(mS/cm^2)$	0.25 [21, 23]	4 [21, 23]
$g_{Kv4.2}(mS/cm^2)$	0.2 [21, 23]	0.2 [21, 23]
$g_{BKCa}(mS/cm^2)$	0.18 [21, 23]	0.3 [21, 23]
$g_{KDR}(mS/cm^2)$	0.01 [21, 23]	0.01 [21, 23]
$g_{Ca_v1.2}(mS/cm^2)$	2 [21, 23]	0.8 [21, 23]
$g_{Ca_v2.1}(mS/cm^2)$	0.1×10^{-2} [21]	0.05×10^{-2} [21]
$g_{Piezo2}(mS/cm^2)$	3 [7]	3 [7]
$g_{Na,leak}(mS/cm^2)$	0.043(Tuned)	0.045(Tuned)
$g_{K,leak}(mS/cm^2)$	0.09(Tuned)	0.09(Tuned)
$g_{Cl,leak}(mS/cm^2)$	0.5×10^{-2} (Tuned)	0.5×10^{-2} (Tuned)
$g_{Ca,leak}(mS/cm^2)$	0.2×10^{-4} (Tuned)	0.2×10^{-4} (Tuned)
$P_{NaKpump}(mol/(cm^2 \cdot ms))$	0.37312×10^{-12} [68]	0.1696×10^{-12} [68]
$P_{NKCC1}(cm^{10}/(mol^3 \cdot ms))$	0.24×10^2 (Tuned)	0.24×10^2 (Tuned)
$P_{KCC2}(mol/(cm^2 \cdot ms))$	0.25×10^{-14} [48, 69]	0.25×10^{-14} [48, 69]
$P_{Capump}(mol/(cm^2 \cdot ms))$	0.3×10^{-15} [22]	$150 * 0.3 \times 10^{-15}$ [24]
$P_{Cana}(mol/(cm^2 \cdot ms))$	0.1×10^{-12} [22, 23]	0.1×10^{-12} [22, 23]
$P_{pump,ER}(mol/(cm^2 \cdot ms))$	0.7×10^{-17} [22, 23]	0.7×10^{-17} [22, 23]
$P_{RYR}(cm/ms)$	8.5 [22, 23]	8.5 [22, 23]
$P_{leak}(cm/ms)$	0.7×10^{-3} (Tuned)	0.7×10^{-3} (Tuned)
$P_{IP_3}(cm/ms)$	1.75 [22, 23]	1.75 [22, 23]
$P_{MCU}(mol/(cm^2 \cdot ms))$	0.5×10^{-15} (Tuned)	0.5×10^{-15} (Tuned)
$P_{MNCX}(mol/(cm^2 \cdot ms))$	0.1×10^{-15} (Tuned)	0.1×10^{-15} (Tuned)

<https://doi.org/10.1371/journal.pcbi.1011720.t003>

constants of Ca^{2+} channels on ER to zero, we can simulate a similar dramatic drop of Ca^{2+} concentration(Fig 4D).

Hypotonic shock. The hypotonic shock also results in Ca^{2+} transients in Merkel cells. Merkel cells were cultured in solutions that remove a part of Na^+ and add the same concentration of mannitols. Then hypotonic shock was induced by removing mannitols in solutions [22, 23]. The hypotonic shock induces Ca^{2+} to enter the cell, and the fluorescence intensity of Ca^{2+} increase slowly, after reaching a peak, Ca^{2+} concentration goes back to the baseline(Fig 5A) [22]. In the simulation, hypotonic shock causes the opening of *Piezo2* channels, Ca^{2+} concentration increases and reaches the peak, then gradually decreases(Fig 5B). But Ca^{2+} transients in the experiments of [22] increase slowly while the Ca^{2+} transients in the simulation have an immediate increase. An important reason is that hypotonic shock can inhibit the cytoplasmic substances' mobility [70], which hinders the quick entry of Ca^{2+} into the cell and diffusion of Ca^{2+} in the cell. However, our model didn't take this inhibitory role of hypotonic shock into account, which is a limitation of our model.

Effects of ion channels properties on membrane potentials and Ca^{2+} transients

According to experiments from [21–24], Merkel cells in different locations of skin, different animals, or different experimental conditions have different expression of ions channels. For example, in experiments of yamashita [21], currents across $K_v1.4$ and $K_v4.2$ channels with inactivation property are dominated in total K^+ currents. While in experiments of piskorowski

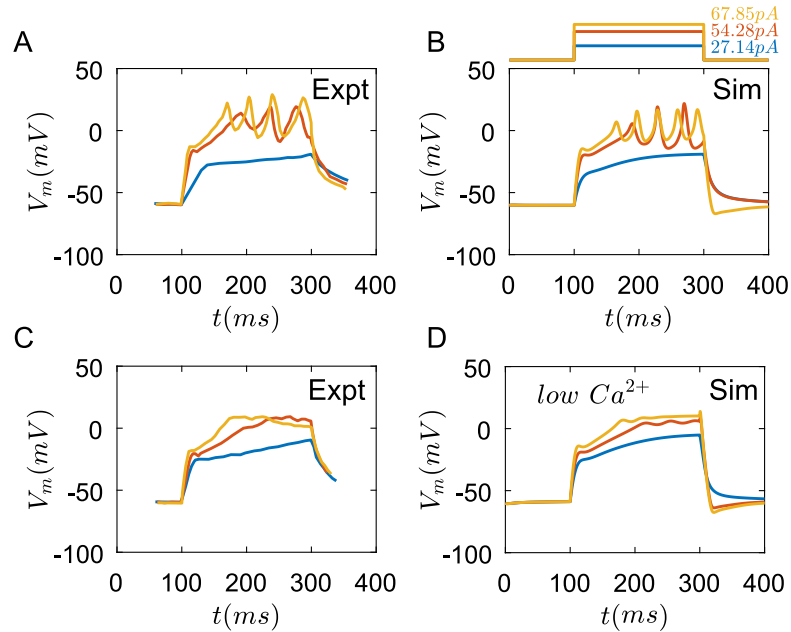


Fig 3. The membrane potential dynamics of one Merkel cell with different properties under the rectangular current pulses. (A) The changes of membrane potential of experimental results from [24]. (B) Membrane potentials change under current pulses in simulation, (C) The changes of membrane potential under the condition of reduced Ca^{2+} concentration in external solutions from [24]. (D) Membrane potentials change under current pulses in simulation at $C_{Ca,out} = 5\mu M$. blue line: 27.14pA, red line: 54.28pA, yellow line: 67.85pA. The parameters of ion channels are seen in Table 3.

<https://doi.org/10.1371/journal.pcbi.1011720.g003>

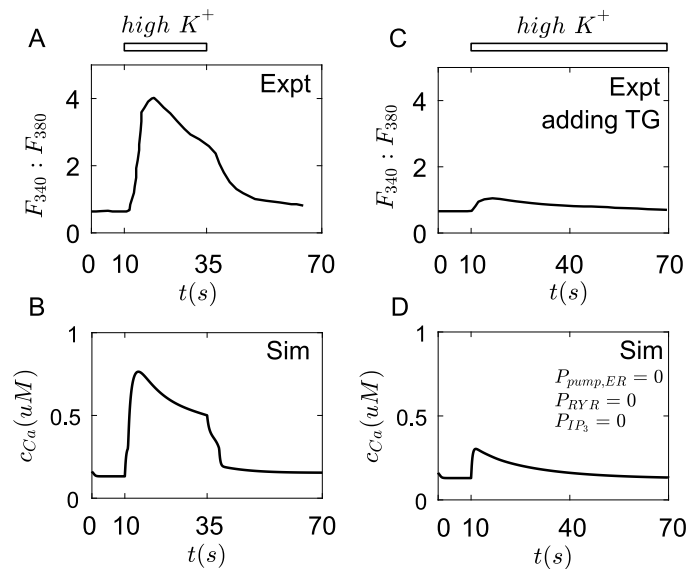


Fig 4. The Ca^{2+} transients in Merkel cells under high K^+ stimulation. (A) The fluorescence intensity change of Ca^{2+} under high K^+ solution [23]. (B) The cytoplasm concentration of Ca^{2+} change under high K^+ solution: $c_{K,out}$ increases by 130nM and $c_{Na,out}$ reduces by 130nM in simulation. (C) The fluorescence intensity change of Ca^{2+} under high K^+ solution by adding thapsigargin (TG), which is a specific blocker of Ca^{2+} pumps on ER, to deplete intracellular Ca^{2+} stores [23]. (D) The cytoplasm concentration of Ca^{2+} change under high K^+ solution in simulation by setting $P_{RYR} = 0$, $P_{leak} = 0$, $P_{IP_3} = 0$, and $P_{pump,ER} = 0$. The parameters of ion channels are seen in Table A in S1 Appendix.

<https://doi.org/10.1371/journal.pcbi.1011720.g004>

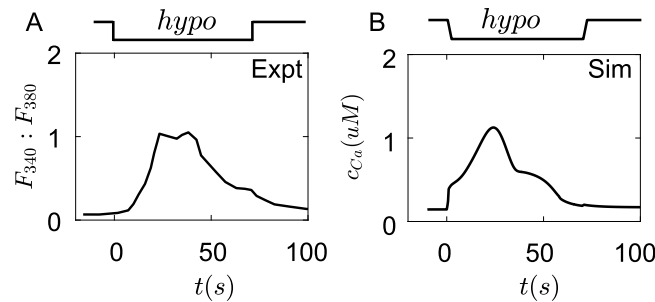


Fig 5. The Ca^{2+} transients in Merkel cells under hypotonic shock. (A) The fluorescence intensity change of Ca^{2+} under hypotonic shock by removing $30mM$ mannitol in external solution [22]. (B) The cytoplasm concentration of Ca^{2+} changes under hypotonic shock by removing $30mM$ mannitol in external solution in simulation. The parameters of ion channels are seen in Table A in S1 Appendix.

<https://doi.org/10.1371/journal.pcbi.1011720.g005>

[23], *BKCa* channels carry 50 ~ 80% of total K^+ currents. The currents only have a slight decrease with time. Therefore, it is reasonable that these channels have various conductances in different Merkel cells. The results from different experiments and our simulation results are consistent with the opinion that these ion channels and pumps in Merkel cells are the keys that regulate the dynamics of membrane potentials and Ca^{2+} transients. However, how these channels control the membrane potentials and Ca^{2+} transients is still unclear.

Membrane potentials. First, we study how Ca^{2+} channels regulate the membrane potentials of Merkel cells. By changing the specific membrane conductance of $Ca_v1.2$ channels, we find that, when $g_{Ca_v1.2}$ is zero, the membrane potential rapidly increases initially, then reaches a steady state gradually. There is no sharp peak for membrane potential (Fig 6A yellow line). With the increase of $g_{Ca_v1.2}$, the membrane potential rapidly rises to its peak. After a small drop, the membrane potential gradually stabilizes (Fig 6A purple line). The peak value of membrane potentials increases with $g_{Ca_v1.2}$ (Fig 6A).

Compared to $Ca_v1.2$ channels, $Ca_v2.1$ channels have little role in the peak form of membrane potentials. When $g_{Ca_v2.1}$ is small, they almost do not affect the membrane potentials (Fig

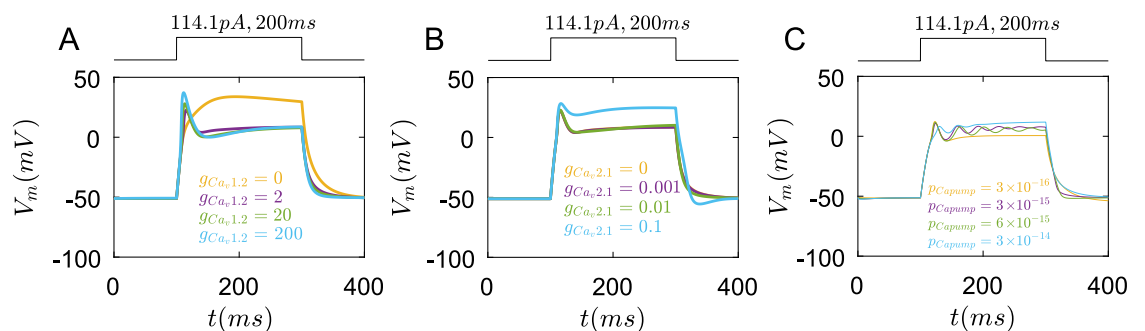


Fig 6. The roles of $Ca_v1.2$, $Ca_v2.1$ channels, and Ca^{2+} pumps in membrane potential regulation under the rectangular current pulse (114.1pA, 200ms). (A) The changes of membrane potential with different $g_{Ca_v1.2}$, yellow line: $g_{Ca_v1.2} = 0$, purple line: $g_{Ca_v1.2} = 2$, green line: $g_{Ca_v1.2} = 20$, blue line: $g_{Ca_v1.2} = 200(mS/cm^2)$. (B) The changes of membrane potential with different $g_{Ca_v2.1}$, yellow line: $g_{Ca_v2.1} = 0$, purple line: $g_{Ca_v2.1} = 0.001$, green line: $g_{Ca_v2.1} = 0.01$, blue line: $g_{Ca_v2.1} = 0.1(mS/cm^2)$. (C) The changes of membrane potential with different P_{Capump} , yellow line: $P_{Capump} = 3 \times 10^{-16}$, purple line: $P_{Capump} = 3 \times 10^{-15}$, green line: $P_{Capump} = 6 \times 10^{-15}$, blue line: $P_{Capump} = 3 \times 10^{-14}(mol/(cm^2 \cdot ms))$.

<https://doi.org/10.1371/journal.pcbi.1011720.g006>

6B). As $g_{Ca_v,2.1}$ increases to 0.1, the membrane potential has a higher steady value(Fig 6B blue line).

However, the phenomenon of membrane potential fire(oscillation) does not happen whatever $g_{Ca_v,1.2}$ or $g_{Ca_v,2.1}$ changes. Interestingly, the oscillations of membrane potentials only appear when p_{Capump} is in the right range (Fig 6C purple and green line). When p_{Capump} is out of the range, the membrane potentials reach a steady state (Fig 6C yellow and blue line).

Next, we study the roles of K^+ channels on membrane potentials. As $g_{K_v,1.4}$ is zero, the membrane potential has a bigger peak(Fig 7A yellow line). With the increase of $g_{K_v,1.4}$, the peak value of membrane potentials decreases(Fig 7A). This result indicates that $K_v1.4$ channels inhibit the peak of membrane potentials caused by Ca^{2+} channels.

As $g_{K_v,4.2}$ is zero or small, they have little influence on membrane potentials(Fig 7B yellow line). This also means that $K_v1.4$ channels mainly regulate the membrane potential peak in normal situations. As $g_{K_v,4.2}$ increases to 20, $K_v4.2$ channels greatly reduce the resting membrane potential, further suppressing the action potential peak(Fig 7B blue line).

When g_{BKCa} is zero, the membrane potential reaches the normal peak but continues to increase over 100mV(Fig 7C yellow line). As g_{BKCa} increases, the membrane potentials decrease to a steady state after reaching the peak(Fig 7C). The steady value of membrane potentials decreases with the increase of g_{BKCa} (Fig 7C).

When g_{KDR} is zero, the membrane potentials have a little change(Fig 7D yellow line). This result also indicates that $BKCa$ channels mainly control the steady membrane potentials. As g_{KDR} increases, the steady membrane potentials also reduce(Fig 7D).

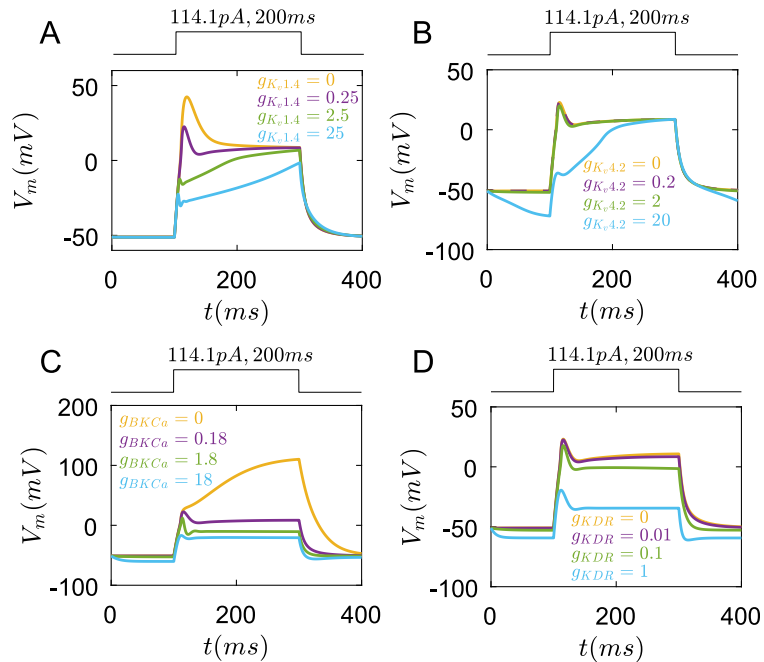


Fig 7. The roles of $K_v1.4$, $K_v4.2$, $BKCa$, and KDR channels in membrane potential regulation under the rectangular current pulse(114.1pA,200ms). (A) The changes of membrane potential with different $g_{K_v,1.4}$. yellow line: $g_{K_v,1.4} = 0$, purple line: $g_{K_v,1.4} = 0.25$, green line: $g_{K_v,1.4} = 2.5$, blue line: $g_{K_v,1.4} = 25(mS/cm^2)$. (B) The changes of membrane potential with different $g_{K_v,4.2}$. yellow line: $g_{K_v,4.2} = 0$, purple line: $g_{K_v,4.2} = 0.2$, green line: $g_{K_v,4.2} = 2$, blue line: $g_{K_v,4.2} = 20(mS/cm^2)$. (C) The changes of membrane potential with different g_{BKCa} . yellow line: $g_{BKCa} = 0$, purple line: $g_{BKCa} = 0.18$, green line: $g_{BKCa} = 1.8$, blue line: $g_{BKCa} = 18(mS/cm^2)$. (D) The changes of membrane potential with different g_{KDR} . yellow line: $g_{KDR} = 0$, purple line: $g_{KDR} = 0.01$, green line: $g_{KDR} = 0.1$, blue line: $g_{KDR} = 1(mS/cm^2)$.

<https://doi.org/10.1371/journal.pcbi.1011720.g007>

In experiments of [21], the inhibition of K^+ channels and the enhancement of Ca^{2+} channels by the external solution containing Ba^{2+} make Merkel cells depolarize at smaller currents injection. This is consistent with our results that with the decrease of conductances of K^+ channels like $K_{v1.4}$, $BKCa$, and KDR channels, the depolarized membrane potentials are more positive (Fig 7A, 7C and 7D). The membrane potentials also form the peak at smaller currents injection, which is consistent with the increase of $g_{Ca_v1.2}$ and the decrease of $g_{K_{v1.4}}$ cause the peak of membrane potentials in simulation (Figs 6A and 7A).

Finally, we also study the influences of internal Ca^{2+} receptors and channels on membrane potentials. However, they almost have no function on membrane potentials (Fig 8).

Together, these results indicate that $Ca_v1.2$ channels mainly help to form the peak of membrane potentials while $K_{v1.4}$ channels directly reduce this peak. The coupling between $Ca_v2.1$, $Ca_v1.2$ channels, and Ca^{2+} pumps contribute to the oscillation of membrane potentials. $BKCa$ and K_{KDR} channels are mainly to maintain a lower steady membrane potential.

Ca²⁺ transients. First, when $g_{Ca_v1.2}$ is zero, cytoplasmic Ca^{2+} concentration only increases slightly under current stimulation (Fig 9A yellow line). As $g_{Ca_v1.2}$ increases, cytoplasmic Ca^{2+} concentration has a rapid rise and fall (Fig 9A). The peak of c_{Ca} increases with $g_{Ca_v1.2}$.

When $g_{Ca_v2.1}$ is zero, they don't affect Ca^{2+} transients (Fig 9B). As $g_{Ca_v1.2}$ increases, the Ca^{2+} concentration not only has a bigger peak but also keeps at a high level for a longer time (Fig 9B green line). However, if $g_{Ca_v2.1}$ increases to 0.002, the Ca^{2+} concentration rises over to $50\mu M$

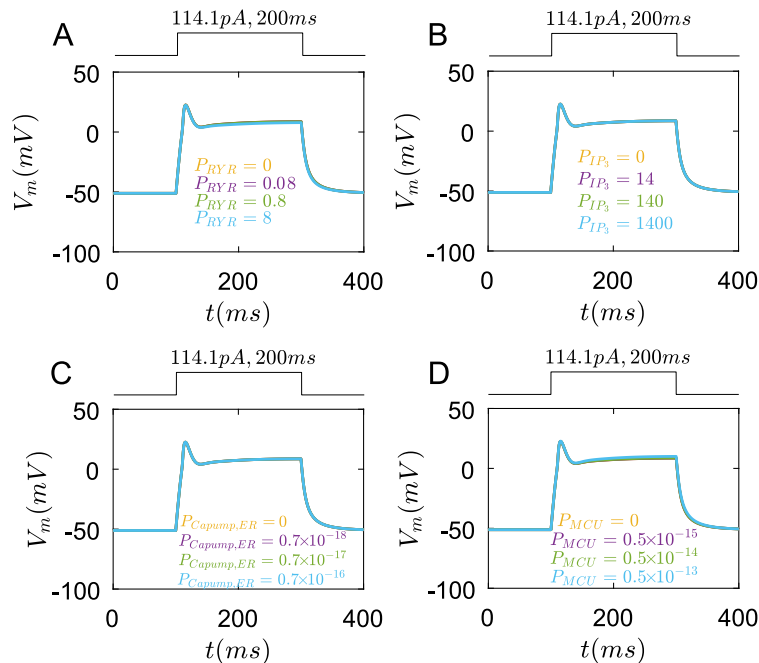


Fig 8. The roles of Ryanodine receptors, IP_3 receptors, ER Ca^{2+} pumps and MCU pumps in membrane potential regulation under the rectangular current pulse (114.1 pA, 200 ms). (A) The changes of membrane potential with different P_{RyR} . yellow line: $P_{RyR} = 0$, purple line: $P_{RyR} = 0.08$, green line: $P_{RyR} = 0.8$, blue line: $P_{RyR} = 8$ (cm/ms). (B) The changes of membrane potential with different P_{IP_3} . yellow line: $P_{IP_3} = 0$, purple line: $P_{IP_3} = 14$, green line: $P_{IP_3} = 140$, blue line: $P_{IP_3} = 1400$ (cm/ms). (C) The changes of membrane potential with different $P_{Capump,ER}$. yellow line: $P_{Capump,ER} = 0$, purple line: $P_{Capump,ER} = 0.7 \times 10^{-18}$, green line: $P_{Capump,ER} = 0.7 \times 10^{-17}$, blue line: $P_{Capump,ER} = 0.7 \times 10^{-16}$ (mol/(cm²·ms)). (D) The changes of membrane potential with different P_{MCU} ($P_{MCU}/P_{MNCX} = 5$). yellow line: $P_{MCU} = 0$, purple line: $P_{MCU} = 0.5 \times 10^{-15}$, green line: $P_{MCU} = 0.5 \times 10^{-14}$, blue line: $P_{MCU} = 0.5 \times 10^{-13}$ (mol/(cm²·ms)).

<https://doi.org/10.1371/journal.pcbi.1011720.g008>

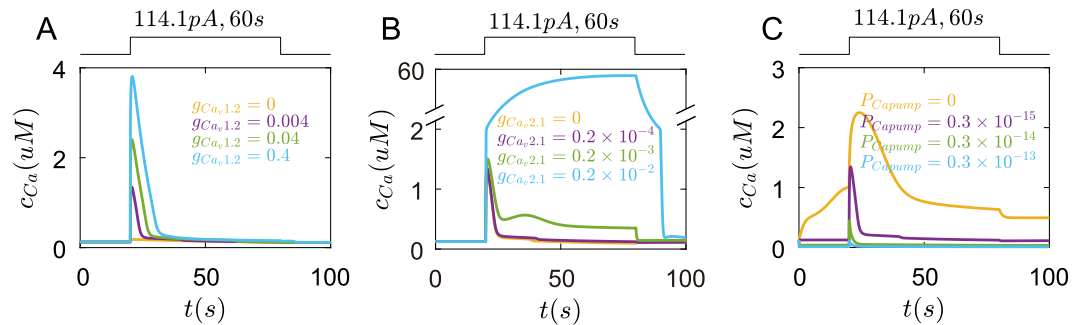


Fig 9. The roles of $Ca_v1.2$, $Ca_v2.1$ channels, and Ca^{2+} pumps in Ca^{2+} transients under the rectangular current pulse (114.1 pA, 60s). (A) The changes of Ca^{2+} concentration in the cell with different $g_{Ca_v1.2}$, yellow line: $g_{Ca_v1.2} = 0$, purple line: $g_{Ca_v1.2} = 0.004$, green line: $g_{Ca_v1.2} = 0.04$, blue line: $g_{Ca_v1.2} = 0.4$ (mS/cm^2). (B) The changes of Ca^{2+} concentration in the cell with different $g_{Ca_v2.1}$, yellow line: $g_{Ca_v2.1} = 0$, purple line: $g_{Ca_v2.1} = 0.2 \times 10^{-4}$, green line: $g_{Ca_v2.1} = 0.2 \times 10^{-3}$, blue line: $g_{Ca_v2.1} = 0.2 \times 10^{-2}$ (mS/cm^2). (C) The changes of Ca^{2+} concentration in the cell with different P_{Capump} , yellow line: $P_{Capump} = 0$, purple line: $P_{Capump} = 0.3 \times 10^{-15}$, green line: $P_{Capump} = 0.3 \times 10^{-14}$, blue line: $P_{Capump} = 0.3 \times 10^{-13}$ ($mol/(cm^2 \cdot ms)$).

<https://doi.org/10.1371/journal.pcbi.1011720.g009>

(Fig 9B blue line), which less happens in normal condition. These results are consistent with the results that the inhibition of $Ca_v1.2$ or $Ca_v2.1$ reduces the Ca^{2+} transients in experiments of [12].

Oppositely, when P_{Capump} is zero, the resting Ca^{2+} concentration is high (Fig 9C yellow line), and the Ca^{2+} transients elicited by the current pulse are more obvious. As P_{Capump} increases, the resting Ca^{2+} concentration gets smaller, and Ca^{2+} transients are also weak (Fig 9C).

Next, $K_v1.4$ and $K_v4.2$ channels both have a little role in Ca^{2+} transients (Fig 10A and 10B).

When g_{BKCa} is zero, the Ca^{2+} concentration rapidly rises to a peak, then enters a long recovery process (Fig 10C yellow line). As g_{BKCa} increases to 0.18, the Ca^{2+} concentration reaches a bigger peak (Fig 10C purple line). But when g_{BKCa} increase to 1.8, the peak of Ca^{2+} concentration decreases. If g_{BKCa} is big enough, the Ca^{2+} transients are inhibited (Fig 10C green and blue line).

When KDR is zero or small, they have little role in the changes of Ca^{2+} concentration (Fig 10D). Only g_{KDR} is big enough, the Ca^{2+} concentration has a very slight increase (Fig 10D blue line).

Finally, the internal Ca^{2+} stores have an obvious impact on Ca^{2+} transients. As P_{RYR} is small, the Ca^{2+} transients are almostly unchanged (Fig 11A yellow line). When P_{RYR} is big, the Ca^{2+} concentration rises to a bigger peak (Fig 11A blue line).

When P_{IP_3} is small, they also do not alter the Ca^{2+} transients (Fig 11B yellow and purple line). This indicates that the Ca^{2+} concentration increase at the beginning of the current stimulus is mostly controlled by $Ca_v1.2$ and $Ca_v2.1$. As P_{IP_3} increases to 140, the Ca^{2+} transients sustain for a longer time (Fig 11B green line). If P_{IP_3} is big enough, the Ca^{2+} concentration has a bigger peak (Fig 11B blue line).

The ER Ca^{2+} pumps have a slight role in Ca^{2+} transients (Fig 11C).

When P_{MCU} is zero, the peak of Ca^{2+} concentration is bigger than the normal situation (Fig 11D yellow line). As P_{MCU} increases, the peak of Ca^{2+} concentration decreases but the duration of Ca^{2+} transients increases (Fig 11D).

Together, these results indicate that $Ca_v1.2$ and $Ca_v2.1$ channels, Ryanodine and IP_3 receptors could increase the Ca^{2+} transients, while $BKCa$ and KDR channels reduce the Ca^{2+} transients. Combining the inhibition roles of $BKCa$ and KDR on membrane potentials, it can be

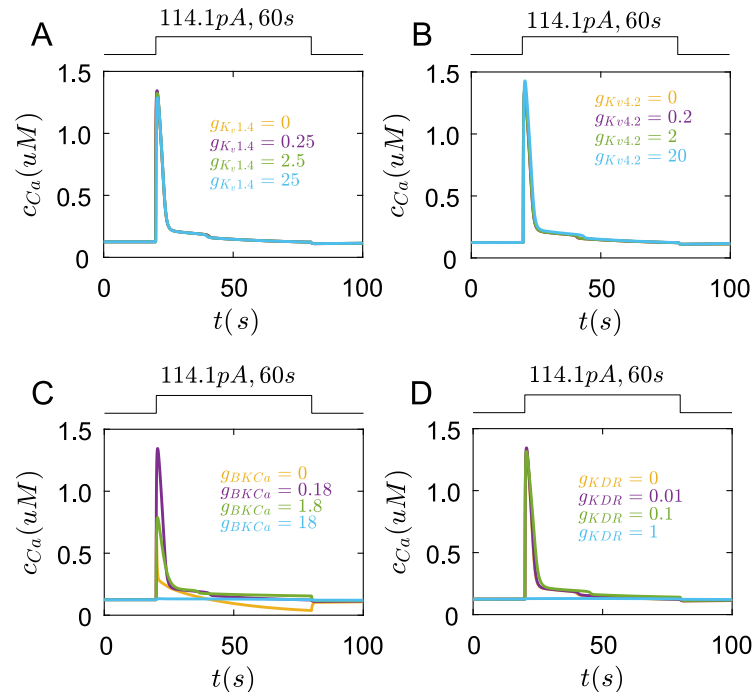


Fig 10. The roles of $K_{v1.4}$, $K_{v4.2}$, $BKCa$ and KDR channels in Ca^{2+} transients under the rectangular current pulse (114.1 pA, 60s). (A) The changes of Ca^{2+} concentration in the cell with different $g_{K_{v1.4}}$: yellow line: $g_{K_{v1.4}} = 0$, purple line: $g_{K_{v1.4}} = 0.25$, green line: $g_{K_{v1.4}} = 2.5$, blue line: $g_{K_{v1.4}} = 25 (mS/cm^2)$. (B) The changes of Ca^{2+} concentration in the cell with different $g_{K_{v4.2}}$: yellow line: $g_{K_{v4.2}} = 0$, purple line: $g_{K_{v4.2}} = 0.2$, green line: $g_{K_{v4.2}} = 2$, blue line: $g_{K_{v4.2}} = 20 (mS/cm^2)$. (C) The changes of Ca^{2+} concentration in the cell with different g_{BKCa} : yellow line: $g_{BKCa} = 0$, purple line: $g_{BKCa} = 0.18$, green line: $g_{BKCa} = 1.8$, blue line: $g_{BKCa} = 18 (mS/cm^2)$. (D) The changes of Ca^{2+} concentration in the cell with different g_{KDR} : yellow line: $g_{KDR} = 0$, purple line: $g_{KDR} = 0.01$, green line: $g_{KDR} = 0.1$, blue line: $g_{KDR} = 1 (mS/cm^2)$.

<https://doi.org/10.1371/journal.pcbi.1011720.g010>

speculated that $BKCa$ and KDR channels, by controlling the resting membrane potentials, further regulate the voltage-gated Ca^{2+} channels to influence the Ca^{2+} transients. $K_{v1.4}$ and $K_{v4.2}$ channels only influence membrane potentials at the initial time, which have less role in Ca^{2+} transients. In turn, the depolarization of membrane potentials facilitates the Ca^{2+} channels also regulate membrane potentials. Therefore, the membrane potentials and the Ca^{2+} transients in Merkel cells are coupled to each other.

How Merkel cells respond to mechanical stimulus

We have studied how ion channels on Merkel cells shape the cell membrane potentials and Ca^{2+} transients. However, Merkel cells are mechanical sensory cells, which could transduce tactile stimuli to SA1 afferents [6, 8, 24]. $Piezo2$ channels are necessary for this transduction [7, 9]. The SA1 afferents generate continuous action potentials under a static mechanical displacement. Without Merkel cells, SA1 afferents only generate action potentials at the initial moment of stimulation. The knockdown of $Piezo2$ channels in the Merkel cells causes similar results. A recent study held the view that $Piezo2$ channels in Merkel cells are not enough to help SA1 afferents generate continuous action potentials [11]. Therefore, we want to know how $Piezo2$ channels and other ion channels in Merkel cells participate in this process. The model is modified as follows.

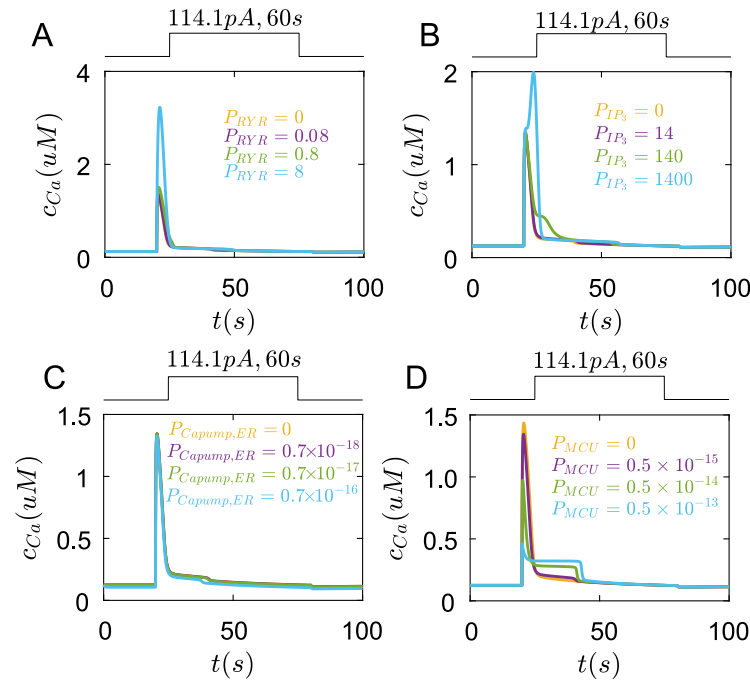


Fig 11. The roles of Ryanodine receptors, IP_3 receptors, ER Ca^{2+} pumps and MCU pumps in Ca^{2+} transients under the rectangular current pulse(114.1pA,200ms). (A) The changes of Ca^{2+} concentration in the cell with different P_{RYR} . yellow line: $P_{RYR} = 0$, purple line: $P_{RYR} = 0.08$, green line: $P_{RYR} = 0.8$, blue line: $P_{RYR} = 8(cm/ms)$. (B) The changes of membrane potential with different P_{IP_3} . yellow line: $P_{IP_3} = 0$, purple line: $P_{IP_3} = 14$, green line: $P_{IP_3} = 140$, blue line: $P_{IP_3} = 1400(cm/ms)$. (C) The changes of Ca^{2+} concentration in the cell with different $P_{Capump,ER}$. yellow line: $P_{Capump,ER} = 0$, purple line: $P_{Capump,ER} = 0.7 \times 10^{-18}$, green line: $P_{Capump,ER} = 0.7 \times 10^{-17}$, blue line: $P_{Capump,ER} = 0.7 \times 10^{-16}(mol/(cm^2 \cdot ms))$. (D) The changes of Ca^{2+} concentration in the cell with different $P_{MCU}(P_{MCU}/P_{MNCX} = 5)$. yellow line: $P_{MCU} = 0$, purple line: $P_{MCU} = 0.5 \times 10^{-15}$, green line: $P_{MCU} = 0.5 \times 10^{-14}$, blue line: $P_{MCU} = 0.5 \times 10^{-13}(mol/(cm^2 \cdot ms))$.

<https://doi.org/10.1371/journal.pcbi.1011720.g011>

Exocytosis and endocytosis. Merkel cells transmit information to downstream afferents by releasing neurotransmitters [15, 16]. Generally, the synapse release can be divided into three parts. First, cell organelles synthesize neurotransmitters into vesicles. Many vesicles form the vesicles pools in the presynapse [71, 72]. Second, When Ca^{2+} ions enter the cell or cytoplasm Ca^{2+} concentration increases, vesicles in the pools fuse to the cell membrane(exocytosis) and release neurotransmitters [15, 16]. Finally, vesicles fused to the membrane recycle into the cell by endocytosis [73, 74]. Vesicles in the pools keep a relatively fixed number at rest, and the consumption of vesicles can be rapidly replenished. Then we assume that the vesicle synthesis rate is inversely related to the number of vesicles. The exocytosis rate increases with the cytoplasm Ca^{2+} concentration [20], and is positively correlated with the number of vesicles. Thus the dynamic equation of vesicles can be written as

$$\frac{dn_{ve}}{dt} = \frac{k_{ve}}{1 + \exp\left(-\frac{n_{ve} - n_{ve,s}}{n_{ve,f}}\right)} - \frac{k_{exo}}{1 + \exp\left(-\frac{c_{Ca} - c_{Ca,s}}{c_{Ca,f}}\right)} n_{ve}, \tag{86}$$

where n_{ve} is the number of vesicles, k_{ve} and k_{exo} are the rate constants. $n_{ve,s}$, $n_{ve,f}$, $c_{Ca,s}$ and $c_{Ca,f}$ are constants.

Endocytosis is regulated by many complex signals, one of which is membrane tension [75–77]. Generally, when the membrane tension is great, more energy is required for vesicles to form from the cell membrane. Therefore, the endocytosis rate can take the form of $\frac{k_{endo}}{1 + \exp\left(\frac{\sigma - \sigma_{s,ve}}{\sigma_{f,ve}}\right)}$ [77, 78], where k_{endo} is rate constant. $\sigma_{s,ve}$ and $\sigma_{f,ve}$ are constants. Endocytosis reduces the cell membrane, while exocytosis adds the cell membrane. Thus the reference surface S_{ref} changes as

$$\frac{dS_{ref}}{dt} = 4\pi r_{ve}^2 \left(\frac{k_{exo}}{1 + \exp\left(-\frac{c_{Ca} - c_{Ca,s}}{c_{Ca,f}}\right)} n_{ve} - \frac{k_{endo}}{1 + \exp\left(\frac{\sigma - \sigma_{s,ve}}{\sigma_{f,ve}}\right)} \right), \tag{87}$$

where r_{ve} is the average radius of vesicles. The values of parameters are seen in Table 4.

Cell compression. The Merkel cell is a sphere before indentation, it is compressed to a cylinder of changeable radius r as shown in Fig A in S1 Appendix. It’s height H decreases with compression depth d ,

$$H = 2r_{ini} - d, \tag{88}$$

where r_{ini} is the initial cell radius before compression. The other equations about the cell deformation are seen in Cell indentation in S1 Appendix.

The results show that when the Merkel cell was compressed(Fig 12A), the shape change of the cell causes the increase of cortex stress σ (Fig 12B), further activates *Piezo2* channels(Fig 12C), Ca^{2+} flow through *Piezo2* channels into the cell, which causes the depolarization of membrane potential(Fig 12D). The increase of membrane potential opens $Ca_v2.1$ and $Ca_v1.2$ channels(Fig 12E and 12F). The Ca^{2+} flow across *Piezo2*, $Ca_v2.1$, and $Ca_v1.2$ channels results in the increase of Ca^{2+} concentration(Fig 12G), further promoting exocytosis (Fig 12H). Then vesicles in the cell decrease (Fig 12I). Cytoplasmic Ca^{2+} further cause the Ca^{2+} release in the ER(Fig 12J).

Piezo2 channels inactivate rapidly under compression(Fig 12C). Without currents of *Piezo2* channels, the membrane potentials repolarize(Fig 12H). It is consistent with the results of [7]. Voltage-gated $Ca_v2.1$ and $Ca_v1.2$ channels also close(Fig 12H). The Ca^{2+} concentration starts to decrease slowly(Fig 12G). With the increase of compression depth d_0 , the depolarization of membrane potential is enhanced, and the rise of Ca^{2+} concentration strengthens.

Table 4. Parameters of endocytosis and exocytosis.

Parameter	Description	Value in simulation
k_{ve}	Vesicle forming rate (1/ms)	0.1 [79]
$n_{ve,s}$	Reference vesicles number (1)	500 [66, 80]
$n_{ve,f}$	Reference vesicles number (1)	50 [66, 80]
k_{exo}	Exocytosis rate constant (1/ms)	2×10^{-4} [75, 81]
$c_{Ca,s}$	Reference Ca^{2+} concentration (μM)	0.2 [82]
$c_{Ca,f}$	Reference Ca^{2+} concentration (μM)	0.01 [82]
r_{ve}	Vesicles radius (μm)	0.05 [66]
k_{endo}	Endocytosis rate constant (1/ms)	1 [75, 78, 80]
$\sigma_{ve,s}$	Reference cortex stress (Pa)	1000 [78]
$\sigma_{ve,f}$	Reference cortex stress (Pa)	15 [78]

<https://doi.org/10.1371/journal.pcbi.1011720.t004>

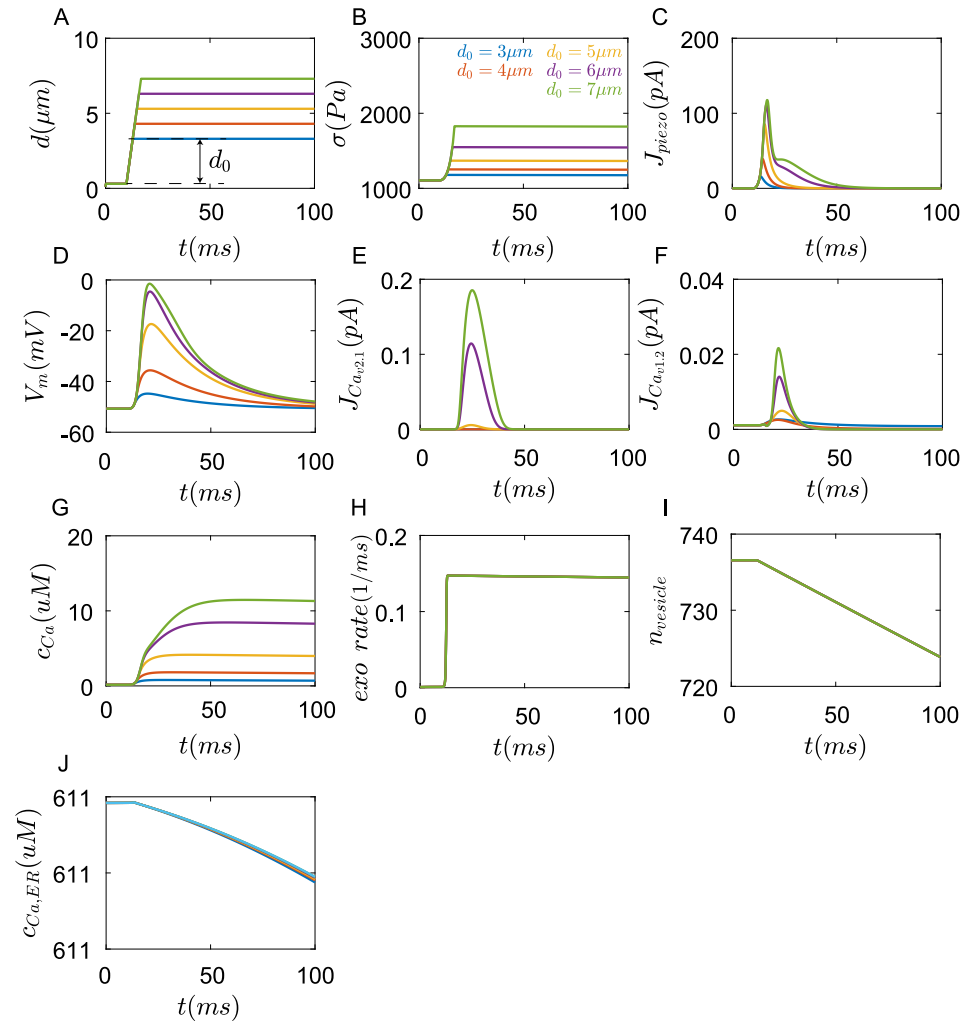


Fig 12. Responses of Merkel cells under compression in 100ms. (A) The Merkel cell was compressed at a depth d_0 with a speed of $1\mu\text{m}/\text{ms}$. The dynamic change of (B) cortex stress, (C) currents generated in the *Piezo2* channels, (D) membrane potential, (E) currents generated in $\text{Ca}_v2.1$ channels, (F) currents generated in $\text{Ca}_v1.2$ channels, (G) cytoplasmic concentration of Ca^{2+} , (H) exocytosis rate, (I) number of cytoplasmic vesicles, and (J) Endoplasmic reticulum concentration of Ca^{2+} (blue: $d_0 = 3\mu\text{m}$, red: $d_0 = 4\mu\text{m}$, yellow: $d_0 = 5\mu\text{m}$, cyan: $d_0 = 6\mu\text{m}$, green: $d_0 = 7\mu\text{m}$).

<https://doi.org/10.1371/journal.pcbi.1011720.g012>

The above process happens in 100ms. After that, the concentration of Ca^{2+} continue to fall (Fig 13D), but the internal Ca^{2+} stores start to work. The Ca^{2+} in the ER enters the cell through Ryanodine and IP_3 receptors, keeping a relatively high Ca^{2+} concentration, and continuously facilitating exocytosis to release neurotransmitters. Exocytosis can last for tens of seconds. If we assume that neurotransmitters in every vesicle are close. Then the downstream afferents will receive continuous and stable neurotransmitter stimuli, which could generate continuous action potentials. The time of exocytosis increases with the compression depth, which is consistent with the results that the firing time of SAI Afferents increases with the indentation depth in experiments of [6, 7]. However, if *Piezo2* channels were inhibited, no Ca^{2+} currents flow into the cell, and the membrane potential is at rest, Merkel cells will not respond to mechanical stimuli (Fig G in S1 Appendix), which is consistent with the results that the

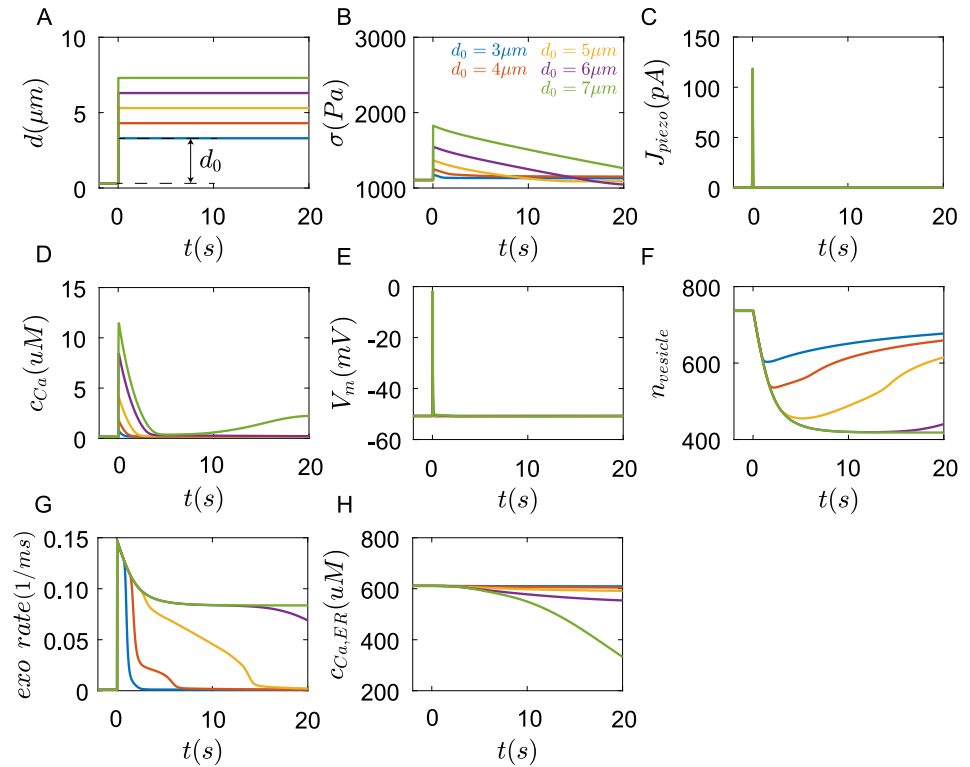


Fig 13. Responses of Merkel cells under compression in 20s. (A) The Merkel cell was compressed at a depth d_0 with a speed of $1\mu\text{m}/\text{ms}$. The dynamic change of (B) cortex stress, (C) currents generated in the *Piezo2* channels, (D) membrane potential, (E) cytoplasmic concentration of Ca^{2+} , (F) number of cytoplasmic vesicles, (G) exocytosis rate, and (H) Endoplasmic reticulum concentration of Ca^{2+} (blue: $d_0 = 3\mu\text{m}$, red: $d_0 = 4\mu\text{m}$, yellow: $d_0 = 5\mu\text{m}$, cyan: $d_0 = 6\mu\text{m}$, green: $d_0 = 7\mu\text{m}$).

<https://doi.org/10.1371/journal.pcbi.1011720.g013>

knockout of *Piezo2* channel or inhibitory of *Piezo2* channels by Ca^{2+} result in the loss of sustained action potentials in the SAI afferents [7, 24].

Discussion

In this article, we develop a biophysically detailed model of Merkel cells for the reception of Merkel cells. We first validate our model of Merkel cells with previous experiments. We then discuss how these ion channels control the membrane potentials and Ca^{2+} transients in Merkel cells. Finally, we study how Merkel cells convert the mechanical stimuli into the release of neurotransmitters with the participation of *Piezo2* channels, membrane potentials, and Ca^{2+} transients.

The responses of Merkel cells under different stimuli

First, the membrane potentials of Merkel cells are controlled by K^+ and Ca^{2+} channels. As shown in Fig 2, Merkel cells exhibit a nearly passive response under small current stimuli. As the injection currents increase, the membrane potential forms a peak and then has a small decrease to the steady state. How do K^+ and Ca^{2+} contribute to this phenomenon? As the conductances of $K_{V1.4}$, $BKCa$, and KDR decrease, the depolarized membrane potential increases, which is consistent with the results that Merkel cells are easier to depolarize with the inhibition

of K^+ channels [21]. Oppositely, the increase of the conductances of Ca^{2+} channels increases the peak of membrane potentials, which is also similar to the results that the membrane potentials form a peak with the small currents stimulus when Ca^{2+} channels were enhanced [21]. Ca^{2+} also can contribute to the oscillation of membrane potentials. As shown in Fig 3, The membrane potentials of Merkel cells initially have a rapid depolarization, then gradually enter an oscillation. By reducing the Ca^{2+} concentration in the external solution, this oscillation disappears [24]. In simulation, by changing the conductance of Ca^{2+} pumps, there is also the oscillation of membrane potentials. Though there are different Ca^{2+} -relative membrane potentials behaviors in Merkel cells. However, it seems to have no obvious qualitative influence on the mechanical transduction of Merkel cells. The action potentials of downstream SAI afferents with two kinds of membrane potentials are still similar [7, 24]. There may be other roles for the oscillation of membrane potentials of Merkel cells, which needs further study. On the other hand, the oscillation of membrane potentials of Merkel cells is smaller than the amplitude of action potentials of neural cells. The membrane potentials are still limited on low depolarization state by K^+ channels.

Secondly, a high K^+ solution is a general way to stimulate Merkel cells, for the main K^+ channels expressed in the cell membrane. High K^+ solutions alter the Nernst potentials of K^+ , which causes the flow of K^+ into the cell, and the membrane depolarizes. The Ca^{2+} channels were opened, and Ca^{2+} enter the cell. Ca^{2+} transients were inspired. This process both link with membrane Ca^{2+} channels and internal Ca^{2+} stores. The inhibition of internal Ca^{2+} stores greatly reduce the amplitude of Ca^{2+} transients(Fig 4), which is consistent with the results in [23]. The decrease of the conductances of $Ca_v1.2$ and $Ca_v2.1$ channels also reduces the Ca^{2+} transients(Fig 9), with is consistent with that the inhibition of $Ca_v1.2$ and $Ca_v2.1$ reduces the Ca^{2+} transients in experiments of [12].

Finally, the hypotonic shock also causes the Ca^{2+} transients(Fig 5), different from the previous two stimuli, hypotonic shock is more like a mechanical stimulus. Piezo2 channels were opened with the increase of cortex stress for the water absorption of the cell. The membrane potential increases, and Ca^{2+} enters the cell. It can be seen that the differences of Ca^{2+} transients between experiments [22] and simulation(Fig 5). The Ca^{2+} concentration in the simulation almost immediately increases, then gradually rises to the peak. However, in the experiments of [22, 23], the Ca^{2+} transients at the beginning of stimulation increase slowly, then rise and fall. One of the possible reasons is that hypotonic shock can inhibit the cytoplasmic substances' mobility [70], thus hindering the quick entry of Ca^{2+} into the cell and the diffusion of Ca^{2+} in the cell. However, this role of hypotonic shock has not been confirmed, which is a limitation of our model.

How Merkel cells with Piezo2 channels help $A\beta$ afferents generate sustained action potentials

According to our model, when Merkel cells are compressed, the opening of Piezo2 channels leads to the depolarization of membrane potentials and the influx of Ca^{2+} . The increase of membrane potential further causes the influx of Ca^{2+} through $Ca_v1.2$ and $Ca_v2.1$. Ca^{2+} in the cytoplasm causes the exocytosis of neurotransmitters. Due to the rapid inactivation of Piezo2 channels, the membrane potential goes back to the resting state within hundreds of milliseconds. The Ca^{2+} channels are also closed. The concentration of Ca^{2+} in the cytoplasm decreases. But the internal Ca^{2+} store begins to release Ca^{2+} into the cell, which can last for tens of seconds. Exocytosis lasts for the same amount of time until Ca^{2+} transients disappear. Therefore, Piezo2 channels excite Merkel cells to produce a sustained neurotransmitter release, which further helps $A\beta$ generate prolonged action potentials. So why does the theoretical study of [11]

have such a conclusion that RA MS channels like *Piezo2* channels cannot account for the sustained responses of Merkel cell-neurite complexes? Because they treat Merkel cells as ordinary nerve cells. A typical feature of these kinds of cells like afferents is that they generate Na^+ -related action potentials. For typical nerve cells, an action potential travels through axons and arrives at the presynapse, which depolarizes the presynaptic membrane potential. Then voltage-gated Ca^{2+} channels on the presynaptic membrane are opened, allowing Ca^{2+} to enter the cell and activate neurotransmitters release [83, 84]. But the Ca^{2+} transients in these nerve cells quickly return to the baseline [32, 85]. The number of vesicles released is positively correlated with the number of arriving action potentials. Therefore, the action potentials of downstream nerve cells are also positively related to the action potentials of presynapse [86–88]. If the nerve cell is compressed, the opening of *Piezo2* channels will only make one or several action potentials [46]. Therefore, the misuse of neural properties in Merkel cells leads to the wrong conclusion [11].

Limitations of the model

Merkel cell-neurite complexes generate sustained action potentials with irregular intervals when a sustained mechanical stimulus is applied to the skin [3, 6, 7, 24]. This irregular interval of action potentials is also one of the important features of the SA1 response. At least in our results, the neurotransmitter release of one Merkel cell is regular. There are at least two aspects that may lead to this phenomenon. First, not only Ca^{2+} , IP_3 , but also many other secondary messengers like ATP and cAMP, play important roles in exocytosis in many neurons [89–92]. These secondary messengers interact with each other, regulating the irregular exocytosis, which further contributes to the irregular intervals. Secondly, an afferent is usually linked with several Merkel cells [8, 93, 94]. It means that even if a single Merkel cell releases vesicles regularly, the combination of several or dozens of Merkel cells with small differences in channel properties may lead to irregularities in the whole action potentials. The research of [93] found that the different locations in the skin, cell size, and so on of Merkel cells may determine this irregular interval. Modeling virtual Merkel cells by different membrane capacitance, and different conductance of ion channels also helps downstream afferents generate irregular action potentials. Therefore, further studies on this irregular action potential are needed.

In this article, we didn't consider the diffusion of Ca^{2+} and IP_3 in the cytoplasm due to the rather small size of Merkel cells. However, the diffusion of Ca^{2+} may cause the Ca^{2+} wave within the cell. This means that the Ca^{2+} concentration in the cytoplasm will be nonuniform, which may lead to more complex Ca^{2+} behaviors. In previous studies, the Ca^{2+} transients in the same cell by two same stimuli can be different [22, 23].

Although the *Piezo2* channels prefer Ca^{2+} , Ca^{2+} in external solutions is much smaller than Na^+ and K^+ . These two kinds of cation channels also flux through *Piezo2* channels. Here we ignore ions other than Ca^{2+} in *Piezo2* channels. It may have quantitative impacts on our results.

Generally speaking, neurotransmitters in vesicles are adequate. But for Merkel cells, the release of neurotransmitters lasts for tens of seconds, and the supplements of vesicles and neurotransmitters may need to be considered. Upon stimulation, the neurotransmitters released in the synapse and vesicles fused to the membrane will be absorbed back into the cell, and some of the neurotransmitters will also diffuse into adjacent solutions [75, 95, 96]. The time scales of reabsorption of neurotransmitters and vesicles may be out of sync. There is even a “kiss and run” approach to neurotransmitter release, where neurotransmitters are released into the synaptic cleft but the membrane of vesicles goes back to the cell immediately.

Therefore, the recycling of neurotransmitters and vesicles may also influence the sustained response of Merkel cells to stimulation.

Conclusion

Although it has been identified that Merkel cells transduce tactile stimuli to SA1 afferents by *Piezo2* channels, it remains unclear how *Piezo2* channels with fast-inactivation properties help Merkel cells and SA1 afferents generate a slowly adapting response to mechanical stimuli. Here, we develop a biophysically detailed model for the reception of Merkel cells.

We first validate our model with several experimental results [21–24]. Merkel cells exhibit an almost passive response to negative current and small positive current pulses. As the positive current increases, the membrane potential rises to a peak value and then gradually reaches a steady state. Merkel cells also exhibit Ca^{2+} transients lasting tens of seconds under high K^+ solutions and hypotonic shock.

We then discuss how these ion channels control the membrane potentials and Ca^{2+} transients in Merkel cells. Our works show that $Ca_v1.2$ channels contribute to the formation of the peak of membrane potentials, while $K_v1.4$ channels reduce this peak. $Ca_v2.1$, *BKCa*, and *KDR* channels mainly maintain the steady membrane potentials, $Ca_v2.1$ channels increase the steady membrane potentials, and *BKCa* and *KDR* channels reduce the steady membrane potentials. Interestingly, the oscillations of membrane potentials require the coupling of Ca^{2+} channels and Ca^{2+} pumps. Compared to these channels on the membrane, the Ryanodine and IP_3 receptors on ER have little role in membrane potentials. Our works also show that $Ca_v1.2$ channels increase the peak concentrations of Ca^{2+} , while $Ca_v2.1$ channels mainly increase the duration of high Ca^{2+} concentrations. Both *BKCa* and *KDR* channels suppress the Ca^{2+} transients. It can be speculated that these two channels inhibit the depolarization of membrane potentials, thereby inhibiting the voltage-gated Ca^{2+} channels on the membrane. Additionally, both Ryanodine and IP_3 receptors on ER increase the Ca^{2+} transients.

Finally, we show that *Piezo2* channels and internal Ca^{2+} stores are sufficient to activate continuous neurotransmitter release to downstream $A\beta$ afferents. Surprisingly, the membrane potentials seem not necessary for Merkel cells to transduce mechanical stimuli to afferents. The depolarization of membrane potentials caused by *Piezo2* channels will rapidly repolarize for the inactivation of *Piezo2* channels. Oppositely, Ca^{2+} flows into the cell through *Piezo2* channels, which activates Ryanodine and IP_3 receptors on ER to keep a continuous high Ca^{2+} concentration. This Ca^{2+} transients facilitate the release of neurotransmitters, and the duration of exocytosis is corresponding to the time of $A\beta$ afferents firing [6, 7, 24].

Thus, unlike sensory cells that generate Na^+ -related action potentials, Merkel cells, through stable membrane potentials and Ca^{2+} transients regulation, maintain a relatively stable release of neurotransmitters to mechanical stimuli.

However, knowledge about the neurotransmitter interaction between Merkel cells and $A\beta$ afferents is still lacking [97]. In further research, we hope to establish a complete model of the Merkel cell and $A\beta$ afferents, which may provide a better description or understanding of the sensing process of the Merkel cell-neurite complexes.

Supporting information

S1 Appendix. Description of cell indentation and additional informations about this work.

Fig A. The schematic diagram of Merkel cell under indentation. Fig B. $K_v1.4$ channel. Fig C. $K_v4.2$ channel. Fig D. *KDR* channel. Fig E. *Piezo2* channel. Fig F. Merkel cell reaches a balanced state given an initial value at rest. Fig G. The responses of Merkel cells under compression. Fig H. The responses of the Merkel cell under three kinds of stimuli with the same parameters. Fig

I. The influences of exocytosis rate on vesicle regulation. Table A. Ion channel parameters in high K^+ solutions and hypotonic shock. Table B. Ion concentrations of external solutions. Table C. Initial values of variables.

(PDF)

S1 Data. Code data of the model in this work.

(ZIP)

Acknowledgments

We thanks Yuehua Yang and Jinjiang Xie for modeling and discussion of results.

Author Contributions

Conceptualization: Fangtao Mao, Wenzhen Yang.

Data curation: Fangtao Mao.

Formal analysis: Fangtao Mao, Wenzhen Yang.

Funding acquisition: Fangtao Mao, Wenzhen Yang.

Investigation: Fangtao Mao, Wenzhen Yang.

Methodology: Fangtao Mao, Wenzhen Yang.

Project administration: Wenzhen Yang.

Resources: Fangtao Mao, Wenzhen Yang.

Software: Fangtao Mao.

Supervision: Wenzhen Yang.

Validation: Fangtao Mao, Wenzhen Yang.

Visualization: Fangtao Mao, Wenzhen Yang.

Writing – original draft: Fangtao Mao, Wenzhen Yang.

Writing – review & editing: Fangtao Mao, Wenzhen Yang.

References

1. Iggo A, Muir AR. The structure and function of a slowly adapting touch corpuscle in hairy skin. *The Journal of physiology*. 1969; 200(3):763. <https://doi.org/10.1113/jphysiol.1969.sp008721> PMID: 4974746
2. Johansson RS, Flanagan JR. Coding and use of tactile signals from the fingertips in object manipulation tasks. *Nature Reviews Neuroscience*. 2009; 10(5):345–359. <https://doi.org/10.1038/nrn2621> PMID: 19352402
3. Abaira VE, Ginty DD. The sensory neurons of touch. *Neuron*. 2013; 79(4):618–639. <https://doi.org/10.1016/j.neuron.2013.07.051> PMID: 23972592
4. Johnson KO, Yoshioka T, Vega-Bermudez F. Tactile functions of mechanoreceptive afferents innervating the hand. *Journal of Clinical Neurophysiology*. 2000; 17(6):539–558. <https://doi.org/10.1097/00004691-200011000-00002> PMID: 11151974
5. Goodwin A, Browning A, Wheat H. Representation of curved surfaces in responses of mechanoreceptive afferent fibers innervating the monkey's fingerpad. *Journal of Neuroscience*. 1995; 15(1):798–810. <https://doi.org/10.1523/JNEUROSCI.15-01-00798.1995> PMID: 7823181
6. Maksimovic S, Nakatani M, Baba Y, Nelson AM, Marshall KL, Wellnitz SA, et al. Epidermal Merkel cells are mechanosensory cells that tune mammalian touch receptors. *Nature*. 2014; 509(7502):617–621. <https://doi.org/10.1038/nature13250> PMID: 24717432

7. Woo SH, Ranade S, Weyer AD, Dubin AE, Baba Y, Qiu Z, et al. Piezo2 is required for Merkel-cell mechanotransduction. *Nature*. 2014; 509(7502):622–626. <https://doi.org/10.1038/nature13251> PMID: 24717433
8. Woo SH, Lumpkin EA, Patapoutian A. Merkel cells and neurons keep in touch. *Trends in cell biology*. 2015; 25(2):74–81. <https://doi.org/10.1016/j.tcb.2014.10.003> PMID: 25480024
9. Ranade SS, Woo SH, Dubin AE, Moshourab RA, Wetzel C, Petrus M, et al. Piezo2 is the major transducer of mechanical forces for touch sensation in mice. *Nature*. 2014; 516(7529):121–125. <https://doi.org/10.1038/nature13980> PMID: 25471886
10. Jenkins BA, Lumpkin EA. Developing a sense of touch. *Development*. 2017; 144(22):4078–4090. <https://doi.org/10.1242/dev.120402> PMID: 29138290
11. Gerling GJ, Wan L, Hoffman BU, Wang Y, Lumpkin EA. Computation predicts rapidly adapting mechanotransduction currents cannot account for tactile encoding in Merkel cell-neurite complexes. *PLoS computational biology*. 2018; 14(6):e1006264. <https://doi.org/10.1371/journal.pcbi.1006264> PMID: 29958280
12. Haeberle H, Fujiwara M, Chuang J, Medina MM, Panditrao MV, Bechstedt S, et al. Molecular profiling reveals synaptic release machinery in Merkel cells. *Proceedings of the National Academy of Sciences*. 2004; 101(40):14503–14508. <https://doi.org/10.1073/pnas.0406308101> PMID: 15448211
13. Maksimovic S, Baba Y, Lumpkin EA. Neurotransmitters and synaptic components in the Merkel cell–neurite complex, a gentle-touch receptor. *Annals of the New York Academy of Sciences*. 2013; 1279(1):13–21. <https://doi.org/10.1111/nyas.12057> PMID: 23530998
14. Chang W, Kanda H, Ikeda R, Ling J, DeBerry JJ, Gu JG. Merkel disc is a serotonergic synapse in the epidermis for transmitting tactile signals in mammals. *Proceedings of the National Academy of Sciences*. 2016; 113(37):E5491–E5500. <https://doi.org/10.1073/pnas.1610176113> PMID: 27573850
15. Hoffman BU, Baba Y, Griffith TN, Mosharov EV, Woo SH, Roybal DD, et al. Merkel cells activate sensory neural pathways through adrenergic synapses. *Neuron*. 2018; 100(6):1401–1413. <https://doi.org/10.1016/j.neuron.2018.10.034> PMID: 30415995
16. Higashikawa A, Kimura M, Shimada M, Ohyama S, Ofusa W, Tazaki M, et al. Merkel cells release glutamate following mechanical stimulation: implication of glutamate in the Merkel cell–neurite complex. *Frontiers in Cellular Neuroscience*. 2019; 13:255. <https://doi.org/10.3389/fncel.2019.00255> PMID: 31244612
17. Boulais N, Pennec JP, Lebonvallet N, Pereira U, Rougier N, Dorange G, et al. Rat Merkel cells are mechanoreceptors and osmoreceptors. *PloS one*. 2009; 4(11):e7759. <https://doi.org/10.1371/journal.pone.0007759> PMID: 19898622
18. Sun J, Pang ZP, Qin D, Fahim AT, Adachi R, Südhof TC. A dual-Ca²⁺-sensor model for neurotransmitter release in a central synapse. *Nature*. 2007; 450(7170):676–682. <https://doi.org/10.1038/nature06308> PMID: 18046404
19. Hosoi N, Holt M, Sakaba T. Calcium dependence of exo- and endocytotic coupling at a glutamatergic synapse. *Neuron*. 2009; 63(2):216–229. <https://doi.org/10.1016/j.neuron.2009.06.010> PMID: 19640480
20. Wang B, Dudko OK. A theory of synaptic transmission. *Elife*. 2021; 10:e73585. <https://doi.org/10.7554/eLife.73585> PMID: 34970965
21. Yamashita Y, Akaike N, Wakamori M, Ikeda I, Ogawa H. Voltage-dependent currents in isolated single Merkel cells of rats. *The Journal of physiology*. 1992; 450(1):143–162. <https://doi.org/10.1113/jphysiol.1992.sp019120> PMID: 1331421
22. Haeberle H, Bryan LA, Vadakkan TJ, Dickinson ME, Lumpkin EA. Swelling-activated Ca²⁺ channels trigger Ca²⁺ signals in Merkel cells. *PloS one*. 2008; 3(3):e1750. <https://doi.org/10.1371/journal.pone.0001750> PMID: 18454189
23. Piskrowski R, Haeberle H, Panditrao MV, Lumpkin EA. Voltage-activated ion channels and Ca²⁺-induced Ca²⁺ release shape Ca²⁺ signaling in Merkel cells. *Pflügers Archiv-European Journal of Physiology*. 2008; 457:197–209. <https://doi.org/10.1007/s00424-008-0496-3> PMID: 18415122
24. Ikeda R, Cha M, Ling J, Jia Z, Coyle D, Gu JG. Merkel cells transduce and encode tactile stimuli to drive A β -afferent impulses. *Cell*. 2014; 157(3):664–675. <https://doi.org/10.1016/j.cell.2014.02.026> PMID: 24746027
25. Guinard D, Usson Y, Guillermet C, Saxod R. Merkel complexes of human digital skin: Three-dimensional imaging with confocal laser microscopy and double immunofluorescence. *Journal of Comparative Neurology*. 1998; 398(1):98–104. [https://doi.org/10.1002/\(SICI\)1096-9861\(19980817\)398:1%3C98::AID-CNE6%3E3.0.CO;2-4](https://doi.org/10.1002/(SICI)1096-9861(19980817)398:1%3C98::AID-CNE6%3E3.0.CO;2-4) PMID: 9703029
26. Hoffmann EK, Lambert IH, Pedersen SF. Physiology of cell volume regulation in vertebrates. *Physiological reviews*. 2009; 89(1):193–277. <https://doi.org/10.1152/physrev.00037.2007> PMID: 19126758

27. Fraser JA, Huang CLH. A quantitative analysis of cell volume and resting potential determination and regulation in excitable cells. *The Journal of Physiology*. 2004; 559(2):459–478. <https://doi.org/10.1113/jphysiol.2004.065706> PMID: 15243134
28. Hugnot JP, Salinas M, Lesage F, Guillemare E, De Weille J, Heurteaux C, et al. Kv8. 1, a new neuronal potassium channel subunit with specific inhibitory properties towards Shab and Shaw channels. *The EMBO Journal*. 1996; 15(13):3322–3331. <https://doi.org/10.1002/j.1460-2075.1996.tb00697.x> PMID: 8670833
29. Roeper J, Lorra C, Pongs O. Frequency-dependent inactivation of mammalian A-type K⁺ channel KV1.4 regulated by Ca²⁺/calmodulin-dependent protein kinase. *Journal of Neuroscience*. 1997; 17(10):3379–3391. <https://doi.org/10.1523/JNEUROSCI.17-10-03379.1997> PMID: 9133364
30. Blair TA, Roberds SL, Tamkun MM, Hartshorne RP. Functional characterization of RK5, a voltage-gated K⁺ channel cloned from the rat cardiovascular system. *FEBS letters*. 1991; 295(1-3):211–213. [https://doi.org/10.1016/0014-5793\(91\)81420-D](https://doi.org/10.1016/0014-5793(91)81420-D) PMID: 1722463
31. Sweet TB, Cox DH. Measuring the influence of the BKCa β 1 subunit on Ca²⁺ binding to the BKCa channel. *Journal of General Physiology*. 2009; 133(2):139–150. <https://doi.org/10.1085/jgp.200810129> PMID: 19139175
32. Mandge D, Manchanda R. A biophysically detailed computational model of urinary bladder small DRG neuron soma. *PLoS computational biology*. 2018; 14(7):e1006293. <https://doi.org/10.1371/journal.pcbi.1006293> PMID: 30020934
33. Fox A, Nowycky M, Tsien R. Kinetic and pharmacological properties distinguishing three types of calcium currents in chick sensory neurones. *The Journal of physiology*. 1987; 394(1):149–172. <https://doi.org/10.1113/jphysiol.1987.sp016864> PMID: 2451016
34. Tong WC, Choi CY, Karche S, Holden AV, Zhang H, Taggart MJ. A computational model of the ionic currents, Ca²⁺ dynamics and action potentials underlying contraction of isolated uterine smooth muscle. *PloS one*. 2011; 6(4):e18685. <https://doi.org/10.1371/journal.pone.0018685> PMID: 21559514
35. Fukumoto N, Kitamura N, Niimi K, Takahashi E, Itakura C, Shibuya I. Ca²⁺ channel currents in dorsal root ganglion neurons of P/Q-type voltage-gated Ca²⁺ channel mutant mouse, rolling mouse Nagoya. *Neuroscience research*. 2012; 73(3):199–206. <https://doi.org/10.1016/j.neures.2012.04.006> PMID: 22575052
36. Coste B, Mathur J, Schmidt M, Earley TJ, Ranade S, Petrus MJ, et al. Piezo1 and Piezo2 are essential components of distinct mechanically activated cation channels. *Science*. 2010; 330(6000):55–60. <https://doi.org/10.1126/science.1193270> PMID: 20813920
37. Wu J, Lewis AH, Grandl J. Touch, tension, and transduction—the function and regulation of Piezo ion channels. *Trends in biochemical sciences*. 2017; 42(1):57–71. <https://doi.org/10.1016/j.tibs.2016.09.004> PMID: 27743844
38. Lewis AH, Cui AF, McDonald MF, Grandl J. Transduction of repetitive mechanical stimuli by Piezo1 and Piezo2 ion channels. *Cell reports*. 2017; 19(12):2572–2585. <https://doi.org/10.1016/j.celrep.2017.05.079> PMID: 28636944
39. Jiang H, Sun SX. Cellular pressure and volume regulation and implications for cell mechanics. *Biophysical journal*. 2013; 105(3):609–619. <https://doi.org/10.1016/j.bpj.2013.06.021> PMID: 23931309
40. Coste B, Xiao B, Santos JS, Syeda R, Grandl J, Spencer KS, et al. Piezo proteins are pore-forming subunits of mechanically activated channels. *Nature*. 2012; 483(7388):176–181. <https://doi.org/10.1038/nature10812> PMID: 22343900
41. Rugiero F, Drew LJ, Wood JN. Kinetic properties of mechanically activated currents in spinal sensory neurons. *The Journal of physiology*. 2010; 588(2):301–314. <https://doi.org/10.1113/jphysiol.2009.182360> PMID: 19948656
42. Chapman JB, Johnson EA, Kootsey JM. Electrical and biochemical properties of an enzyme model of the sodium pump. *The Journal of membrane biology*. 1983; 74(2):139–153. <https://doi.org/10.1007/BF01870503> PMID: 6308260
43. Apell HJ, Karlsh S. Functional properties of Na, K-ATPase, and their structural implications, as detected with biophysical techniques. *The Journal of membrane biology*. 2001; 180(1):1–9. <https://doi.org/10.1007/s002320010053> PMID: 11284199
44. Armstrong CM. The Na/K pump, Cl ion, and osmotic stabilization of cells. *Proceedings of the National Academy of Sciences*. 2003; 100(10):6257–6262. <https://doi.org/10.1073/pnas.0931278100> PMID: 12730376
45. Bueno-Orovio A, Sánchez C, Pueyo E, Rodríguez B. Na/K pump regulation of cardiac repolarization: insights from a systems biology approach. *Pflügers Archiv-European Journal of Physiology*. 2014; 466(2):183–193. <https://doi.org/10.1007/s00424-013-1293-1> PMID: 23674099

46. Mao F, Yang Y, Jiang H. Electromechanical model for object roughness perception during finger sliding. *Biophysical Journal*. 2022; 121(23):4740–4747. <https://doi.org/10.1016/j.bpj.2022.09.014> PMID: 36116008
47. Currin CB, Trevelyan AJ, Akerman CJ, Raimondo JV. Chloride dynamics alter the input-output properties of neurons. *PLOS Computational Biology*. 2020; 16(5):e1007932. <https://doi.org/10.1371/journal.pcbi.1007932> PMID: 32453795
48. Doyon N, Vinay L, Prescott SA, De Koninck Y. Chloride regulation: a dynamic equilibrium crucial for synaptic inhibition. *Neuron*. 2016; 89(6):1157–1172. <https://doi.org/10.1016/j.neuron.2016.02.030> PMID: 26985723
49. Yellin F, Li Y, Sreenivasan VK, Farrell B, Johnny MB, Yue D, et al. Electromechanics and Volume Dynamics in Nonexcitable Tissue Cells. *Biophysical Journal*. 2018; 114(9):2231–2242. <https://doi.org/10.1016/j.bpj.2018.03.033> PMID: 29742416
50. Delpire E, Days E, Lewis LM, Mi D, Kim K, Lindsley CW, et al. Small-molecule screen identifies inhibitors of the neuronal K-Cl cotransporter KCC2. *Proceedings of the National Academy of Sciences*. 2009; 106(13):5383–5388. <https://doi.org/10.1073/pnas.0812756106> PMID: 19279215
51. Williams JR, Payne JA. Cation transport by the neuronal K⁺-Cl⁻ cotransporter KCC2: thermodynamics and kinetics of alternate transport modes. *American Journal of Physiology-Cell Physiology*. 2004; 287(4):C919–C931. <https://doi.org/10.1152/ajpcell.00005.2004> PMID: 15175220
52. Ellingsrud AJ, Daversin-Catty C, Rognes ME. A cell-based model for ionic electrodiffusion in excitable tissue. *Modeling Excitable Tissue: The EMI Framework*. 2021; p. 14–27. https://doi.org/10.1007/978-3-030-61157-6_2
53. Parekh AB, Putney JW Jr. Store-operated calcium channels. *Physiological reviews*. 2005; 85(2):757–810. <https://doi.org/10.1152/physrev.00057.2003> PMID: 15788710
54. Blaustein MP, Lederer WJ. Sodium/calcium exchange: its physiological implications. *Physiological reviews*. 1999; 79(3):763–854. <https://doi.org/10.1152/physrev.1999.79.3.763> PMID: 10390518
55. Fridlyand LE, Tamarina N, Philipson LH. Modeling of Ca²⁺ flux in pancreatic β -cells: role of the plasma membrane and intracellular stores. *American Journal of Physiology-Endocrinology and Metabolism*. 2003; 285(1):E138–E154. <https://doi.org/10.1152/ajpendo.00194.2002> PMID: 12644446
56. Gall D, Gromada J, Susa I, Rorsman P, Herchuelz A, Bokvist K. Significance of Na/Ca exchange for Ca²⁺ buffering and electrical activity in mouse pancreatic β -cells. *Biophysical Journal*. 1999; 76(4):2018–2028. [https://doi.org/10.1016/S0006-3495\(99\)77359-5](https://doi.org/10.1016/S0006-3495(99)77359-5) PMID: 10096898
57. Luo Ch, Rudy Y. A dynamic model of the cardiac ventricular action potential. I. Simulations of ionic currents and concentration changes. *Circulation research*. 1994; 74(6):1071–1096. <https://doi.org/10.1161/01.RES.74.6.1071> PMID: 7514509
58. Favre CJ, Schrenzel J, Jacquet J, Lew DP, Krause KH. Highly supralinear feedback inhibition of Ca²⁺ uptake by the Ca²⁺ load of intracellular stores. *Journal of Biological Chemistry*. 1996; 271(25):14925–14930. <https://doi.org/10.1074/jbc.271.25.14925> PMID: 8662967
59. Fink CC, Slepchenko B, Moraru II, Watras J, Schaff JC, Loew LM. An image-based model of calcium waves in differentiated neuroblastoma cells. *Biophysical Journal*. 2000; 79(1):163–183. [https://doi.org/10.1016/S0006-3495\(00\)76281-3](https://doi.org/10.1016/S0006-3495(00)76281-3) PMID: 10866945
60. Bezprozvanny I, Watras J, Ehrlich BE. Bell-shaped calcium-response curves of Ins (1, 4, 5) P₃- and calcium-gated channels from endoplasmic reticulum of cerebellum. *Nature*. 1991; 351(6329):751–754. <https://doi.org/10.1038/351751a0> PMID: 1648178
61. Kaftan EJ, Ehrlich BE, Watras J. Inositol 1, 4, 5-trisphosphate (InsP₃) and calcium interact to increase the dynamic range of InsP₃ receptor-dependent calcium signaling. *The Journal of general physiology*. 1997; 110(5):529–538. <https://doi.org/10.1085/jgp.110.5.529> PMID: 9348325
62. Mikoshiba K. The InsP₃ receptor and intracellular Ca²⁺ signaling. *Current opinion in neurobiology*. 1997; 7(3):339–345. [https://doi.org/10.1016/S0959-4388\(97\)80061-X](https://doi.org/10.1016/S0959-4388(97)80061-X) PMID: 9232803
63. Hirose K, Kadowaki S, Tanabe M, Takeshima H, Iino M. Spatiotemporal dynamics of inositol 1, 4, 5-trisphosphate that underlies complex Ca²⁺ mobilization patterns. *Science*. 1999; 284(5419):1527–1530. <https://doi.org/10.1126/science.284.5419.1527> PMID: 10348740
64. Li Wh, Llopis J, Whitney M, Zlokarnik G, Tsien RY. Cell-permeant caged InsP₃ ester shows that Ca²⁺ spike frequency can optimize gene expression. *Nature*. 1998; 392(6679):936–941. <https://doi.org/10.1038/31965> PMID: 9582076
65. McLaughlin S, Wang J, Gambhir A, Murray D. PIP₂ and proteins: interactions, organization, and information flow. *Annual review of biophysics and biomolecular structure*. 2002; 31(1):151–175. <https://doi.org/10.1146/annurev.biophys.31.082901.134259> PMID: 11988466
66. Halata Z, Grim M, Bauman KI. Friedrich Sigmund Merkel and his “Merkel cell”, morphology, development, and physiology: review and new results. *The Anatomical Record Part A: Discoveries in Molecular,*

- Cellular, and Evolutionary Biology: An Official Publication of the American Association of Anatomists. 2003; 271(1):225–239. PMID: [12552639](#)
67. Shutov LP, Kim MS, Houlihan PR, Medvedeva YV, Usachev YM. Mitochondria and plasma membrane Ca²⁺-ATPase control presynaptic Ca²⁺ clearance in capsaicin-sensitive rat sensory neurons. *The Journal of physiology*. 2013; 591(10):2443–2462. <https://doi.org/10.1113/jphysiol.2012.249219> PMID: [23381900](#)
 68. Larsen EH, Møbjerg N, Nielsen R. Application of the Na⁺ recirculation theory to ion coupled water transport in low-and high resistance osmoregulatory epithelia. *Comparative Biochemistry and Physiology Part A: Molecular & Integrative Physiology*. 2007; 148(1):101–116. <https://doi.org/10.1016/j.cbpa.2006.12.039> PMID: [17303459](#)
 69. Doyon N, Prescott SA, De Koninck Y. Mild KCC2 hypofunction causes inconspicuous chloride dysregulation that degrades neural coding. *Frontiers in cellular neuroscience*. 2016; 9:516. <https://doi.org/10.3389/fncel.2015.00516> PMID: [26858607](#)
 70. Konopka MC, Sochacki KA, Bratton BP, Shkel IA, Record MT, Weisshaar JC. Cytoplasmic protein mobility in osmotically stressed *Escherichia coli*. *Journal of bacteriology*. 2009; 191(1):231–237. <https://doi.org/10.1128/JB.00536-08> PMID: [18952804](#)
 71. Kusick GF, Chin M, Raychaudhuri S, Lippmann K, Adula KP, Hujber EJ, et al. Synaptic vesicles transiently dock to refill release sites. *Nature neuroscience*. 2020; 23(11):1329–1338. <https://doi.org/10.1038/s41593-020-00716-1> PMID: [32989294](#)
 72. Denker A, Kröhnert K, Bückers J, Neher E, Rizzoli SO. The reserve pool of synaptic vesicles acts as a buffer for proteins involved in synaptic vesicle recycling. *Proceedings of the National Academy of Sciences*. 2011; 108(41):17183–17188. <https://doi.org/10.1073/pnas.1112690108> PMID: [21903923](#)
 73. Hua Y, Sinha R, Martineau M, Kahms M, Klingauf J. A common origin of synaptic vesicles undergoing evoked and spontaneous fusion. *Nature neuroscience*. 2010; 13(12):1451–1453. <https://doi.org/10.1038/nn.2695> PMID: [21102448](#)
 74. Sankaranarayanan S, Ryan TA. Calcium accelerates endocytosis of vSNAREs at hippocampal synapses. *Nature neuroscience*. 2001; 4(2):129–136. <https://doi.org/10.1038/83949> PMID: [11175872](#)
 75. Wu LG, Hamid E, Shin W, Chiang HC. Exocytosis and endocytosis: modes, functions, and coupling mechanisms. *Annual review of physiology*. 2014; 76:301–331. <https://doi.org/10.1146/annurev-physiol-021113-170305> PMID: [24274740](#)
 76. Doherty GJ, McMahon HT. Mechanisms of endocytosis. *Annual review of biochemistry*. 2009; 78:857–902. <https://doi.org/10.1146/annurev.biochem.78.081307.110540> PMID: [19317650](#)
 77. Dai J, Sheetz M. Regulation of endocytosis, exocytosis, and shape by membrane tension. In: *Cold Spring Harbor symposia on quantitative biology*. vol. 60. Cold Spring Harbor Laboratory Press; 1995. p. 567–571.
 78. Mao F, Yang Y, Jiang H. Endocytosis and exocytosis protect cells against severe membrane tension variations. *Biophysical Journal*. 2021; 120(24):5521–5529. <https://doi.org/10.1016/j.bpj.2021.11.019> PMID: [34838532](#)
 79. Groulx N, Boudreault F, Orlov SN, Grygorczyk R. Membrane reserves and hypotonic cell swelling. *The Journal of membrane biology*. 2006; 214:43–56. <https://doi.org/10.1007/s00232-006-0080-8> PMID: [17598067](#)
 80. van der Wijk T, Tomassen SF, Houtsmuller AB, de Jonge HR, Tilly BC. Increased vesicle recycling in response to osmotic cell swelling: cause and consequence of hypotonicity-provoked ATP release. *Journal of Biological Chemistry*. 2003; 278(41):40020–40025. <https://doi.org/10.1074/jbc.M307603200> PMID: [12871943](#)
 81. Morris C, Homann U. Cell surface area regulation and membrane tension. *The Journal of membrane biology*. 2001; 179:79–102. <https://doi.org/10.1007/s002320010040> PMID: [11220366](#)
 82. Von Gersdorff H, Mathews G. Dynamics of synaptic vesicle fusion and membrane retrieval in synaptic terminals. *Nature*. 1994; 367(6465):735–739. <https://doi.org/10.1038/367735a0> PMID: [7906397](#)
 83. Bostock H, Sears T. The internodal axon membrane: electrical excitability and continuous conduction in segmental demyelination. *The Journal of physiology*. 1978; 280(1):273–301. <https://doi.org/10.1113/jphysiol.1978.sp012384> PMID: [690876](#)
 84. Alle H, Geiger JR. Combined analog and action potential coding in hippocampal mossy fibers. *Science*. 2006; 311(5765):1290–1293. <https://doi.org/10.1126/science.1119055> PMID: [16513983](#)
 85. Delvendahl I, Hallermann S. The cerebellar mossy fiber synapse as a model for high-frequency transmission in the mammalian CNS. *Trends in neurosciences*. 2016; 39(11):722–737. <https://doi.org/10.1016/j.tins.2016.09.006> PMID: [27771145](#)

86. Rancz EA, Ishikawa T, Duguid I, Chadderton P, Mahon S, Häusser M. High-fidelity transmission of sensory information by single cerebellar mossy fibre boutons. *Nature*. 2007; 450(7173):1245–1248. <https://doi.org/10.1038/nature05995> PMID: 18097412
87. Chamberland S, Timofeeva Y, Evstratova A, Volynski K, Tóth K. Action potential counting at giant mossy fiber terminals gates information transfer in the hippocampus. *Proceedings of the National Academy of Sciences*. 2018; 115(28):7434–7439. <https://doi.org/10.1073/pnas.1720659115> PMID: 29946034
88. Spruston N, Schiller Y, Stuart G, Sakmann B. Activity-dependent action potential invasion and calcium influx into hippocampal CA1 dendrites. *Science*. 1995; 268(5208):297–300. <https://doi.org/10.1126/science.7716524> PMID: 7716524
89. Shibasaki T, Sunaga Y, Fujimoto K, Kashima Y, Seino S. Interaction of ATP sensor, cAMP sensor, Ca²⁺ + sensor, and voltage-dependent Ca²⁺ channel in insulin granule exocytosis. *Journal of Biological Chemistry*. 2004; 279(9):7956–7961. <https://doi.org/10.1074/jbc.M309068200> PMID: 14660679
90. Seino S, Shibasaki T. PKA-dependent and PKA-independent pathways for cAMP-regulated exocytosis. *Physiological reviews*. 2005; 85(4):1303–1342. <https://doi.org/10.1152/physrev.00001.2005> PMID: 16183914
91. Ozaki N, Shibasaki T, Kashima Y, Miki T, Takahashi K, Ueno H, et al. cAMP-GEFII is a direct target of cAMP in regulated exocytosis. *Nature cell biology*. 2000; 2(11):805–811. <https://doi.org/10.1038/35041046> PMID: 11056535
92. Xie L, Zhang M, Zhou W, Wu Z, Ding J, Chen L, et al. Extracellular ATP stimulates exocytosis via localized Ca²⁺ release from acidic stores in rat pancreatic β cells. *Traffic*. 2006; 7(4):429–439. <https://doi.org/10.1111/j.1600-0854.2006.00401.x> PMID: 16536741
93. Lesniak DR, Marshall KL, Wellnitz SA, Jenkins BA, Baba Y, Rasband MN, et al. Computation identifies structural features that govern neuronal firing properties in slowly adapting touch receptors. *Elife*. 2014; 3:e01488. <https://doi.org/10.7554/eLife.01488> PMID: 24448409
94. Nakatani M, Maksimovic S, Baba Y, Lumpkin EA. Mechanotransduction in epidermal Merkel cells. *Pflügers Archiv-European Journal of Physiology*. 2015; 467:101–108. <https://doi.org/10.1007/s00424-014-1569-0> PMID: 25053537
95. Südhof TC. Neurotransmitter release: the last millisecond in the life of a synaptic vesicle. *Neuron*. 2013; 80(3):675–690. <https://doi.org/10.1016/j.neuron.2013.10.022> PMID: 24183019
96. Watanabe S, Rost BR, Camacho-Pérez M, Davis MW, Söhl-Kielczynski B, Rosenmund C, et al. Ultra-fast endocytosis at mouse hippocampal synapses. *Nature*. 2013; 504(7479):242–247. <https://doi.org/10.1038/nature12809> PMID: 24305055
97. Eispert AC, Fuchs F, Brandner J, Houdek P, Wladykowski E, Moll I. Evidence for distinct populations of human Merkel cells. *Histochemistry and cell biology*. 2009; 132:83–93. <https://doi.org/10.1007/s00418-009-0578-0> PMID: 19319559